NASA TN D-1436

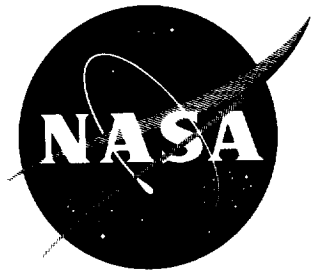

TECHNICAL NOTE
D-1436

HEAT TRANSFER AND PRESSURE DISTRIBUTION ON CONE-CYLINDER-FLARE CONFIGURATION WITH BOUNDARY-LAYER SEPARATION

By Harold Ferguson and John W. Schaefer

Lewis Research Center
Cleveland, Ohio

NATIONAL AERONAUTICS AND SPACE ADMINISTRATION
WASHINGTON
October 1962

NATIONAL AERONAUTICS AND SPACE ADMINISTRATION

TECHNICAL NOTE D-1436

HEAT TRANSFER AND PRESSURE DISTRIBUTION ON CONE-CYLINDER-FLARE CONFIGURATION WITH BOUNDARY-LAYER SEPARATION

By Harold Ferguson and John W. Schaefer

SUMMARY

The heat transfer and the pressure distribution on a cone-cylinder-flare configuration including the separated region across the cylinder-flare junction were measured at a Mach number of 4.98. Results are presented for a 15° half-angle cone-cylinder model in conjunction with conical-flare afterbodies of 10°, 17°, 24°, and 56° half-angles. The unit Reynolds number was varied from 1.6×10^6 to 5.4×10^6 per foot and the wall-temperature ratio from 0.18 to 1.0. Both pure-laminar and transitional separations were observed.

The experimental pressure distributions for attached flow agree favorably with theory. The distribution across the separated region for pure-laminar and transitional separation shows the characteristic rise to a plateau pressure up to the region of the cylinder-flare junction, at which point a steep pressure gradient is initiated.

The heat transfer to the flare depended on the type of separation, pure laminar or transitional. For transitional separation, the heat transfer on the flare was adequately predicted by turbulent theory for an attached boundary layer beginning at the cylinder-flare junction, and peak heating rates occurred in the reattachment region. No peak heating occurred in the reattachment region for pure-laminar separation; the flare heat transfer downstream of reattachment (but upstream of transition) was low but somewhat greater than that predicted by laminar theory.

The extent of pure-laminar and transitional separations decreased with wall cooling, decreasing flare angle, and increasing unit Reynolds number.

INTRODUCTION

The flared surfaces of hypersonic vehicles cause flow characteristics that may seriously influence the surface heat transfer and pressure distribution. Extensive regions of separated flow may be generated that will decrease the vehicle drag and may greatly increase the heat transfer downstream of reattachment. There is, therefore, a need for information on the effects of such variables as body geometry, temperature level, unit Reynolds number, and Mach number on the presence, type, and extent of flow separation and, in turn, the influence of separation on the pressure distribution and heat transfer on a hypersonic vehicle.

The effect of the location of transition on the pressure distribution and heat transfer for separated flows has necessitated some distinction according to types. In reference 1 the flow separation types are classified as (1) pure laminar, where transition occurs downstream of reattachment; (2) transitional, where transition occurs between separation and reattachment; and (3) turbulent, where transition is upstream of separation. In particular, in reference 1, the pressure distribution across a separated region is shown to depend on the type of separation.

The heat transfer in regions of both laminar and turbulent separation has been investigated theoretically for the case of zero or very small boundary-layer thickness at separation (ref. 2). The average heat transfer in the separated region for pure-laminar separation was found for air to be 0.56 of the corresponding value for an attached flow on a solid boundary defined by the edge of the separated region. Reference 3 presents results of an experimental investigation of heat transfer in separated regions that show good agreement with the theory of reference 2 for the average heat transfer for a pure-laminar separation. Both local and average heat-transfer results for pure-laminar and turbulent separations were investigated for bodies approximating the theoretical model of reference 2.

Reference 4 identifies two basic separated-flow regimes, cavity-type separation and wedge-type separation, which exhibit quite different heat-transfer characteristics. (This classification is independent of separation type, pure laminar, transitional, or turbulent; however, pure-laminar separation is considered specifically in ref. 4.) Cavity-type separation is induced by a body cavity whose boundaries at the separation and reattachment points are approximately perpendicular to the flow direction, whereas wedge-type separation is characterized by a small incident angle between the separated flow and the body at the separation and reattachment points. References 2 and 3 concern the heat transfer for cavity-type separations. For this case, the heat transfer for pure-laminar separation was low throughout the separated region. The heat transfer for a laminar wedge-type separation, however,

is reported in reference 4 to have decreased to a minimum near the point of separation and increased considerably thereafter across the remaining separation length. Also, in reference 4, the heat transfer in the attached laminar flow downstream of reattachment was greater than that predicted by laminar theory.

The heat transfer in the reattachment region of a separated flow has generated considerable interest. Experimental results are presented in reference 4 to 7. The experimental reattachment heat-transfer rates reported range from low values that would be associated with a laminar boundary layer to very high values that would be associated with a thin turbulent boundary layer. Consideration of the available results led to the suggestion (ref. 7) that the distinguishing characteristic between the low-reattachment heat-transfer case and the high-reattachment heat-transfer case may be the type of separation.

Reference 8 reports an investigation of the transition Reynolds number for separated flow on an ogive-stepped-cylinder model on which the separation length was controlled. Results are presented for Mach numbers up to 4.24 and for adiabatic- and cold-wall conditions. The transition Reynolds number, based on the length of the separated region, increased with increasing Mach number, unit Reynolds number, and wall temperature.

Reported herein is a study of the heat transfer and pressure distribution on a cone-cylinder-flare configuration, including the separated region. Particular emphasis is placed on the influence of such variables as body geometry, location of transition, wall-temperature ratio, and unit Reynolds number on the type and extent of separation, and, in turn, the influence of separation type on the heat transfer and the pressure distribution. The investigation was conducted at a free-stream Mach number of 4.98 and a free-stream unit Reynolds number range from 1.6×10^6 to 5.4×10^6 per foot. The wall-temperature ratio was varied from 0.18 to 1.0.

APPARATUS AND PROCEDURE

Tests were conducted at the Lewis Research Center in the 1- by 1-foot, Mach 5, variable Reynolds number tunnel at a stagnation temperature of 710° R. The Reynolds number was varied by controlling the plenum pressure. Two series of tests were run: one in which transition occurred naturally, downstream of the point of separation, and another in which transition was induced upstream of the cone-cylinder junction by a boundary-layer trip on the model nose cone.

The model was a conventional cone-cylinder forebody in conjunction with conical-flare afterbodies of 10°, 17°, 24°, and 56° half-angles, as shown in figure 1. The model was made of monel and had a wall thickness of approximately 0.054 inch. The wall thickness at each thermocouple location was measured by an ultrasonic thickness indicator that was calibrated at points on the model wall, where measurements were also made with a ball micrometer. The cylinder-flare junction consisted of mating lips, and the flare was spring-loaded against the cylinder to prevent model separation at the junction and to provide a seal. Figure 2 shows a typical tunnel installation.

In the tripped-boundary-layer series, the trip was located on the nose cone 3 inches from the tip and consisted of a 1/8-inch-wide band of granulated nickel glued to the model with epoxy cement. The average trip roughness height was approximately 0.025 inch. Transition occurred at the trip for unit Reynolds numbers above about 2.0×10^{6} per foot.

Thermocouple and pressure-tap locations are given in figure 1. Model and tunnel static-pressure data were read from photographs of a manometer board. Pressure-distributions were obtained at equilibrium conditions only.

The thermocouples were made from 30-gage copper and constantan wire. Heat-transfer data were obtained by the transient technique presented in reference 9. The model was enclosed in cooling shoes, shown in figure 2, and cooled with liquid nitrogen to an approximately uniform temperature of 120° R before being introduced into the tunnel stream. The method is discussed in reference 10. Continuous transient-temperature data were recorded on a multichannel oscillograph and equilibrium-temperature data were recorded on a digital recorder.

DATA REDUCTION

The heat-transfer data were evaluated using the familiar thin-wall analysis outlined in reference 10. The heat-transfer coefficient, when conduction and radiation are neglected, is given by

$$h = \frac{\rho_b \left(c_p\right)_b \tau_w \frac{dT_w}{dt}}{T_{aw} - T_w} \tag{1}$$

All symbols are defined in the appendix. The specific heat as a function of temperature was obtained from reference 10. The temperatures were determined from the oscillograph records at discrete times with equal

time intervals. The rate of change of temperature with time was determined by differentiation of a five-point quadratic fit of the experimental temperatures. The experimental equilibrium temperatures were used in the evaluation of the heat transfer.

At the lower unit Reynolds numbers ($Re \leq 2.6 \times 10^6$ ft^{-1}), the manometer-system settling time was prohibitive. Therefore, the pressures on the cylinder across the separated region for low unit Reynolds numbers were obtained by fairing a curve from a high-pressure point in the separated region (which should be accurate) to the theoretical value for the attached flow upstream of separation (see fig. 8(a)).

The classification of the separation types observed in this investigation was accomplished from studies of both schlieren photographs and heat-transfer results. When transition was in the immediate vicinity of reattachment, it was difficult to determine the exact location of transition and, therefore, the type of separation. Since transition for these cases appears in the reattachment region, these are classified as transitional separation.

The maximum estimated errors in the basic quantities that appear in the evaluation of the experimental results are:

Wall thickness, percent	±2
Specific heat of wall material, percent	±3
Stagnation pressure, percent	±1
Static pressure (except as noted), percent	±3

The largest sources of possible error in the heat-transfer coefficient (eq. (1)) are the slope of the temperature history and the temperature difference ($T_{aw} - T_w$). The heat-transfer results are, therefore, less accurate at low unit Reynolds numbers, where dT_w/dt is small, and at high wall temperatures, where both dT_w/dt and $T_{aw} - T_w$ are small. The heat-transfer results presented, however, are felt to be accurate within ±20 percent except for those points indicated by a tailed symbol, for which the possible error is greater.

RESULTS AND DISCUSSION

In the discussion that follows, the separation types are identified, and the effects of such variables as wall cooling, body geometry, and unit Reynolds number on the type and length of separation are considered. The effect of separation type and length of separation on the overall pressure distribution and heat transfer is presented. Pressure distribution is discussed with particular reference to that across the separated region. The heat-transfer results for the separated region are presented, and the influence of separation type on the heat transfer to the flared afterbody is discussed. Finally, the

heat transfer to the flares under conditions of transitional separation is compared with that obtained for an attached turbulent boundary layer over the entire model.

It should be noted that, according to the classification of reference 4, all results presented are for wedge-type separations.

Separation Types

The three types of flow separation according to reference 1, are: pure laminar, where transition is downstream of the reattachment point; transitional, where transition is between the separation and reattachment points; and turbulent, where transition is upstream of separation. In this investigation pure-laminar and transitional separations were observed. As mentioned previously, it was difficult in some cases to classify the separation. Because of the large amount of consistent data available at these conditions, however, the limits on separation type presented in the next paragraphs are felt to be reasonably accurate.

Pure-laminar separation, shown in figure 3, was observed only for the minimum flare angle, $\theta = 10^{\circ}$, at unit Reynolds numbers below 2.6×10^6 per foot. As the unit Reynolds number increases, transition on the 10° flare moves upstream to the reattachment region. Transition is in the vicinity of reattachment for unit Reynolds numbers higher than 3.6×10^6 per foot. The separation on the 10° flare configuration is, therefore, classified as transitional for unit Reynolds numbers higher than 3.6×10^6 per foot. The approximate unit Reynolds number range on the 10° flare configuration, 2.6×10^6 to 3.6×10^6 per foot, is the range in which it is difficult to distinguish between a pure-laminar and a transitional separation.

Transitional separation, shown in figure 4, was observed at all unit Reynolds numbers for the 17° and 24° flare configurations, at unit Reynolds numbers above 3.6×10^6 per foot on the 10° flare configuration, and at the one unit Reynolds number (5.4×10^6 ft^{-1}) for which results are available for the 56° flare configuration. The location of transition is in the vicinity of reattachment for all cases of transitional separation on the 10°, 17°, and 24° flare configurations, although, as is apparent from a comparison of the schlieren photographs of figure 4, the location of reattachment moves downstream with increasing separation length. The attached turbulent or transitional boundary layer downstream of reattachment was quite thin. For the 56° flare configuration, transition occurred shortly downstream of the point of separation, which was the cone-cylinder junction (fig. 4(e)). Transition was observed to move upstream, toward the point of separation, with wall cooling.

The model configuration and test conditions were such that no turbulent-separation results were obtained. Transition did not occur naturally in the attached cylinder boundary layer, and in the case of the tripped boundary layer no separation was observed.

Separation Geometry

The variables defining the geometry of the separated region are shown in figure 5. The point of separation S_s was taken as the point at which the boundary layer began to thicken because of separation. The point of reattachment S_r was taken as the intersection of the extension of the line that delineated the edge of the separated region with the flare surface. In all cases, the edge of the separated region was closely defined by a straight line (see figs. 3 and 4).

The length of the separated region varied considerably for the range of variables considered in this investigation (figs. 6(a) and 7(a)). The length of separation decreased with decreasing flare angle and wall temperature and increasing unit Reynolds number. The variation of length of separation with flare angle and unit Reynolds number is presented in figure 6(a). As the unit Reynolds number decreased from 5.4×10^6 to 1.6×10^6 per foot, the length of separation increased by a factor slightly greater than 2. The increase in the length of separation with flare angle is also apparent in figure 6(a). The corresponding plot of the distance to separation is presented in figure 6(b). The distance to separation increased with decreasing flare angle and increasing unit Reynolds number.

Separation lengths for wall temperatures below adiabatic are presented in figure 7(a) for the 24° flare configuration, the only flare angle for which extensive results are available. The length of separation decreased by a factor of about 2 as the wall-temperature ratio was reduced from adiabatic to 0.2. It is apparent from the figure that moderate cooling has very little effect on the length of separation; appreciable reduction occurred only below $T_w/T_{aw} \doteq 0.5$. The available results on the 10° and 17° flares indicated a similar behavior. Although no data were taken, it was observed that the length of separation increased when the wall temperature was increased above adiabatic. In figure 7(b), the distance to the point of separation is shown to increase with increasing wall cooling. The separation length for the 56° flare configuration was independent of wall cooling (results are available at $Re = 5.4\times10^6$ ft^{-1} only).

The separation angle α for the 10°, 17°, and 24° flares was approximately constant at 3° independent of type of separation (pure laminar or transitional), flare angle, unit Reynolds number, and wall cooling. For the 56° flare configuration the separation angle was

constant at approximately 10°, which is also the angle defined by a line connecting the cone-cylinder junction and the trailing edge of the flare.

As discussed previously, transition occurred in the reattachment region for all cases of transitional separation on the 10°, 17°, and 24° flare configurations. It would be expected, therefore, that the Reynolds number based on separation length Re_{ℓ} for these transitional separations would be only slightly higher than a transition Reynolds number for separated flow. The transition Reynolds number Re_{TR} is defined from reference 8 as the maximum Reynolds number, based on the length of the separated region, for which laminar flow exists throughout the separated region. According to figures 6(a) and 7(a), Re_{ℓ} and, therefore, Re_{TR} decreased with wall cooling, decreasing unit Reynolds number, and decreasing flare angle. A decrease with wall cooling and unit Reynolds number is also reported in reference 8 for cavity-type separations (for which flare angle was not a variable), but a direct comparison with the results of reference 8 is not possible because of the higher Mach number at which this investigation was conducted.

Equilibrium pressure distributions for the various configurations, for both transitional and pure-laminar separations, are shown in figure 8. The theoretical cone-cylinder pressure distributions shown for attached flow were obtained from reference 11. In reference 12, it is suggested that the attached-flow pressure distribution for a potential flow should decrease uniformly from a two-dimensional value at the leading edge to the cone value as the flare is traversed downstream. Accordingly, the theoretical wedge and cone-pressure coefficients (ref. 13) are shown for each flare. The theoretical wedge and cone-pressure distributions are also included for a body that approximates the shape of the respective separated regions, $\alpha = 3^{\circ}$ for the 10°, 17°, and 24° flare configurations and $\alpha = 10^{\circ}$ for the 56° flare configuration.

As shown in figures 8(a) to (d), the pressure distribution for the attached flow on the cone-cylinder agreed favorably with theory (except as noted in the section DATA REDUCTION for low unit Reynolds number) until separation began to influence the distribution at a point slightly upstream of the point of separation. Between the start of interaction S_0 and the cylinder-flare junction, the pressure increased above the corresponding attached-flow value, and, as seen particularly in figure 8(b), tended to level off to a plateau pressure upstream of the cylinder-flare junction. The plateau pressure fell between that for a cone and that for a wedge at the approximate angle defined by the edge of the separated region ($\alpha = 3^{\circ}$).

The start of the pressure rise associated with the flared afterbody occurred close to the cylinder-flare junction for separation of the cylinder boundary layer, independent of separation type. This behavior is in contradistinction to the two-dimensional separation results presented in reference 1, in which the pressure rise occurred at reattachment for a pure-laminar separation and at transition for a transitional separation. The pressure rise in the vicinity of the cylinder-flare junction reached a value between that for a wedge and that for a cone for the 17° and 24° flare configurations, and it approached the cone value downstream as expected (ref. 12). For a small flare angle ($\alpha = 10^\circ$), however, no peak was apparent, and the pressure was approximately uniform at the cone value.

The pressure distribution for the 56° flare configuration, presented in figure 8(e), shows good agreement with the theoretical value for a cone defined by the edge of the separated region ($\alpha = 10^\circ$). As discussed previously, the separation was transitional, with transition occurring just downstream of the cone-cylinder junction. The theoretical pressure distribution for attached flow on the cylinder is also shown for comparison.

According to reference 1, the pressure distribution across a separated region is well correlated for pure-laminar separation and for transitional separation up to the start of transition by a plot of $(p/p_0 - 1)\Big/\sqrt{(C_f)_0}$ against $(S/S_0 - 1)\Big/\sqrt{(C_f)_0}$, where the subscript 0 indicates the start of interaction of separation on the pressure distribution. The correlation is presented in figure 9 for the faired separated-region pressure distributions up to the start of the pressure rise in the vicinity of the cylinder-flare junction. The shaded area represents the range of the faired results.

The results of an investigation of the plateau pressure for two-dimensional separations are reported in reference 1 for Mach numbers lower than that used in this investigation. From these results and the Mach number effect determined from the analysis in reference 1, the two-dimensional pressure-plateau parameter $(p/p_0 - 1)\Big/\sqrt{(C_f)_0}$ at Mach 5 may be determined. This computed value is approximately 18, as compared with a value of 21 for the three-dimensional separations of the present investigation (fig. 9).

Heat Transfer

The heat-transfer distributions on the 10° and 24° flare configurations for pure-laminar and transitional separations are presented in figures 10(a) to (d) in terms of the product of the Stanton number and

the square root of the free-stream Reynolds number based on body diameter $St\sqrt{Re_D}$. The laminar-attached-flow theory of reference 14 for the entire model is shown. For the separated-flow region on the 24° flare, shown in figures 10(c) and (d), the laminar-attached-flow theory for a body defined by the edge of the separated region is indicated up to the cylinder-flare junction. For the separated-flow region on the 56° flare configuration (fig. 10(e)), the theoretical, laminar heat transfer up to the start of transition is shown for a body defined by the edge of the separated region; the turbulent theory of reference 15 for the same body is indicated over the remaining portion of the model. The theory of reference 15 for a turbulent boundary layer starting at the cylinder-flare junction is also shown for the 10° and 24° flare configurations. The theoretical lines presented are for an isothermal wall at the theoretical pressure distribution for attached flow on the cone-cylinder and for the cone pressure for the flares except as specifically indicated in the figures. Where possible, the locations of the experimental separation and reattachment points are shown. The effect of wall temperature level on the theoretical, isothermal, laminar heat transfer is indicated in figure 10(a); the experimental results agreed favorably with this trend.

The experimental results for attached flow on the cone-cylinder, shown in figures 10(a) to (d), were consistently higher than theory up to the point of separation. The agreement would be expected to improve if the theory were corrected for the axial wall-temperature distribution, as discussed in reference 10.

Because of the larger possible inaccuracies in the separated-region heat-transfer results, the effects of nonuniform wall temperature, and the limited number of data stations in the separated region, a definitive discussion of the heat transfer in the separated region is not possible. Observations based on careful examination of all available results deserve comment, however. The minimum heat transfer occurred slightly downstream of the separation point, and the region of low heat transfer was quite small compared with the length of the separated region. The heat transfer increased sharply upstream of reattachment or transition. This variation was similar to the laminar wedge-type separation results of references 4 and 5. (In the foregoing discussion, no distinction as to separation type, pure laminar or transitional, is made, since, for the transitional separations of this investigation, the separated boundary layer was laminar up to the reattachment region.)

For the transitional separation on the 56° flare configuration, figure 10(e), the heat transfer on the cylinder upstream of transition was somewhat above laminar theory for an attached flow on a cone defined by the separation angle. Downstream of transition the heat transfer on the cylinder was considerably lower than turbulent theory for an

attached flow on the cone defined by the separation angle. The heat-transfer distribution and the magnitude compared with turbulent attached-flow theory were similar to results obtained in reference 3 for turbulent cavity-type separation.

A comparison of the heat-transfer distributions at reattachment and downstream in a pure laminar separation with those in a transitional separation (figs. 10(a) and 10(b) to (d), respectively) demonstrates the significance of separation type on flare heat transfer. For pure-laminar separation (fig. 10(a)) the heat transfer to the flare was similar in trend to laminar theory, though somewhat higher in magnitude. In reference 4, heat transfer higher than laminar theory was also observed downstream of reattachment for pure-laminar separation. The heat-transfer distribution in the reattachment region (fig. 10(a)) was insensitive to reattachment and reflected the existence of an apparently continuous laminar boundary layer through reattachment, as may be seen in the schlieren photograph (fig. 3).

For transitional separation (figs. 10(b) to (d)), peak heating rates were observed in the reattachment region, and the heat transfer agreed favorably with the theory for a turbulent boundary layer beginning at the cylinder-flare junction. The heating rates reflected the transition to a turbulent boundary layer of small thickness at reattachment, as observed from the schlieren photographs (fig. 4). The flare heat-transfer results for both pure-laminar and transitional separation were in general agreement with those of reference 5.

It is interesting to compare the results for the heat transfer to the flares for transitional separation with those obtained for the turbulent attached flow with negligible separation. Such a comparison is made in figure 11 for the heat transfer to the 24° flare configuration. The theory shown is for a turbulent boundary layer beginning at the flare leading edge. The heat transfer to the flare for tripped flow agreed favorably with the theory and exhibited the same behavior as that for transitional separation. The boundary layer in the vicinity of the flare leading edge for the tripped flow was observed in schlieren photographs to be quite thin, as in transitional separation. Similarity of the heat-transfer results for the two cases might therefore be expected.

CONCLUSIONS

The heat transfer and the pressure distribution on a cone-cylinder-flare configuration were investigated experimentally at a Mach number of 4.98. The following conclusions may be drawn from the results of this study:

1. The length of separation of the laminar boundary layer on the cylinder decreases with wall cooling, decreasing flare angle, and increasing unit Reynolds number.

2. The pressure distributions across the separated region of the laminar boundary layer are well correlated by the correlating parameters presented in NACA Rep. 1356. These parameters are $(p/p_0 - 1)\Big/\sqrt{(C_f)_0}$ and $(S/S_0 - 1)\Big/\sqrt{(C_f)_0}$ where p is the pressure, C_f is the local skin-friction coefficient, S is the surface distance along the model, and the subscript 0 refers to the start of the interaction of separation on the pressure distribution.

3. The heat transfer to the flared afterbody depends on the type of separation, pure-laminar or transitional. Pure-laminar separation exhibits relatively low heat-transfer rates through reattachment. Transitional separation, however, is characterized by high heat-transfer rates in the reattachment region. The flare heat transfer for transitional separation is adequately predicted by the theory for a turbulent boundary layer beginning at the cylinder-flare junction.

Lewis Research Center
National Aeronautics and Space Administration
Cleveland, Ohio, June 23, 1962

APPENDIX - SYMBOLS

C_f	local skin-friction coefficient
C_p	pressure coefficient
c_p	specific heat at constant pressure
D	cylinder diameter
h	heat-transfer coefficient
l	length of separated region
p	pressure
Re	free-stream unit Reynolds number, ft^{-1}
Re_D	free-stream Reynolds number based on cylinder diameter
Re_l	free-stream Reynolds number based on length of separation
S	surface distance along model
St	free-stream Stanton number
T	temperature
t	time
x	axial distance along model
α	separation angle
θ	flare angle
ρ	density
τ_w	wall thickness

Subscripts:

aw	adiabatic wall
b	model material

r	reattachment point
s	separation point
TR	transition point
t	stagnation conditions
w	wall
0	start of interaction of separation on pressure distribution

REFERENCES

1. Chapman, Dean R., Kuehn, Donald M., and Larson, Howard K.: Investigation of Separated Flows in Supersonic and Subsonic Streams with Emphasis on the Effect of Transition. NACA Rep. 1356, 1958. (Supersedes NACA TN 3869.)

2. Chapman, Dean R.: A Theoretical Analysis of Heat Transfer in Regions of Separated Flow. NACA TN 3792, 1956.

3. Larson, Howard K.: Heat Transfer in Separated Flow. Jour. Aero/Space Sci., vol. 26, no. 11, Nov. 1959, pp. 731-738.

4. Bogdonoff, S. M., and Vas, I. R.: Some Experiments on Hypersonic Separated Flows. Preprint no. 2172-61, Am. Rocket Soc., Inc., 1961.

5. Becker, John V., and Korycinski, Peter F.: Heat Transfer and Pressure Distribution at a Mach Number of 6.8 on Bodies with Conical Flares and Extensive Flow Separation. NACA RM L56F22, 1956.

6. Stalder, Jackson R., and Nielson, Helmer V.: Heat Transfer from a Hemisphere-Cylinder Equipped with Flow Separation Spikes. NACA TN 3287, 1954.

7. Crawford, Davis H.: Investigation of the Flow Over a Spiked-Nose Hemisphere-Cylinder at a Mach Number of 6.8. NASA TN D-118, 1959.

8. Larson, Howard K., and Keating, Stephen J., Jr.: Transition Reynolds Numbers of Separated Flows at Supersonic Speeds. NASA TN D-349, 1960.

9. Jack, John R., and Diaconis, Nick S.: Variation of Boundary-Layer Transitions with Heat Transfer on Two Bodies of Revolution at a Mach Number of 3.12. NACA TN 3562, 1955.

10. Jack, John R., and Diaconis, Nick S.: Heat-Transfer Measurements on Two Bodies of Revolution at a Mach Number of 3.12. NACA TN 3776, 1956.

11. Clippinger, R. F., Giese, J. H., and Carter, W. C.: Tables of Supersonic Flows About Cone Cylinders. Pt. I: Surface Data. Rep. 729, Ballistic Res. Labs., Aberdeen Proving Ground, July 1950.

12. Jack, John R.: Theoretical Wave Drags and Pressure Distributions for Axially Symmetric Open-Nose Bodies. NACA TN 2115, 1950.

13. Ames Research Staff: Equations, Tables, and Charts for Compressible Flow. NACA Rep. 1135, 1953. (Supersedes NACA TN 1428.)

14. Reshotko, Eli: Simplified Method for Estimating Compressible Laminar Heat Transfer with Pressure Gradient. NACA TN 3888, 1956.

15. Reshotko, Eli, and Tucker, Maurice: Approximate Calculation of the Compressible Turbulent Boundary Layer with Heat Transfer and Arbitrary Pressure Gradient. NACA TN 4154, 1957.

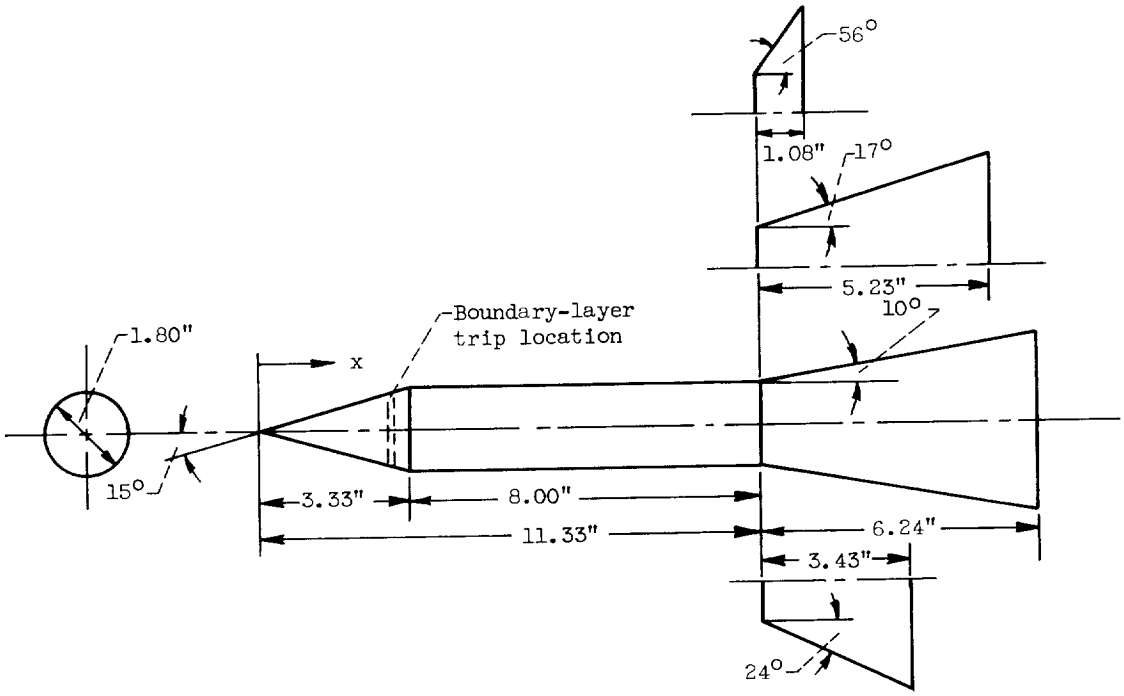

THERMOCOUPLE AND PRESSURE-TAP LOCATIONS

Cone-cylinder	10° Flare	17° Flare	24° Flare	56° Flare
Axial distance along model, x, in.				
1.45	11.39	11.40	11.38	11.37
4.27	11.88	11.88	11.84	11.51
5.27	12.38	12.34	12.30	11.79
6.27	13.04	12.98	12.76	12.06
[a]6.77	13.69	13.61	13.20	12.34
7.27	14.37	14.25	13.65	
[a]7.78	15.01	14.90	14.10	
8.27	15.68	15.53	14.56	
[a]8.78	16.34	16.49		
9.27	16.99			
[a]9.77				
10.27				
10.83				
11.15				

[a]Pressure tap only.

Figure 1. - Model dimensions and thermocouple and pressure-tap locations.

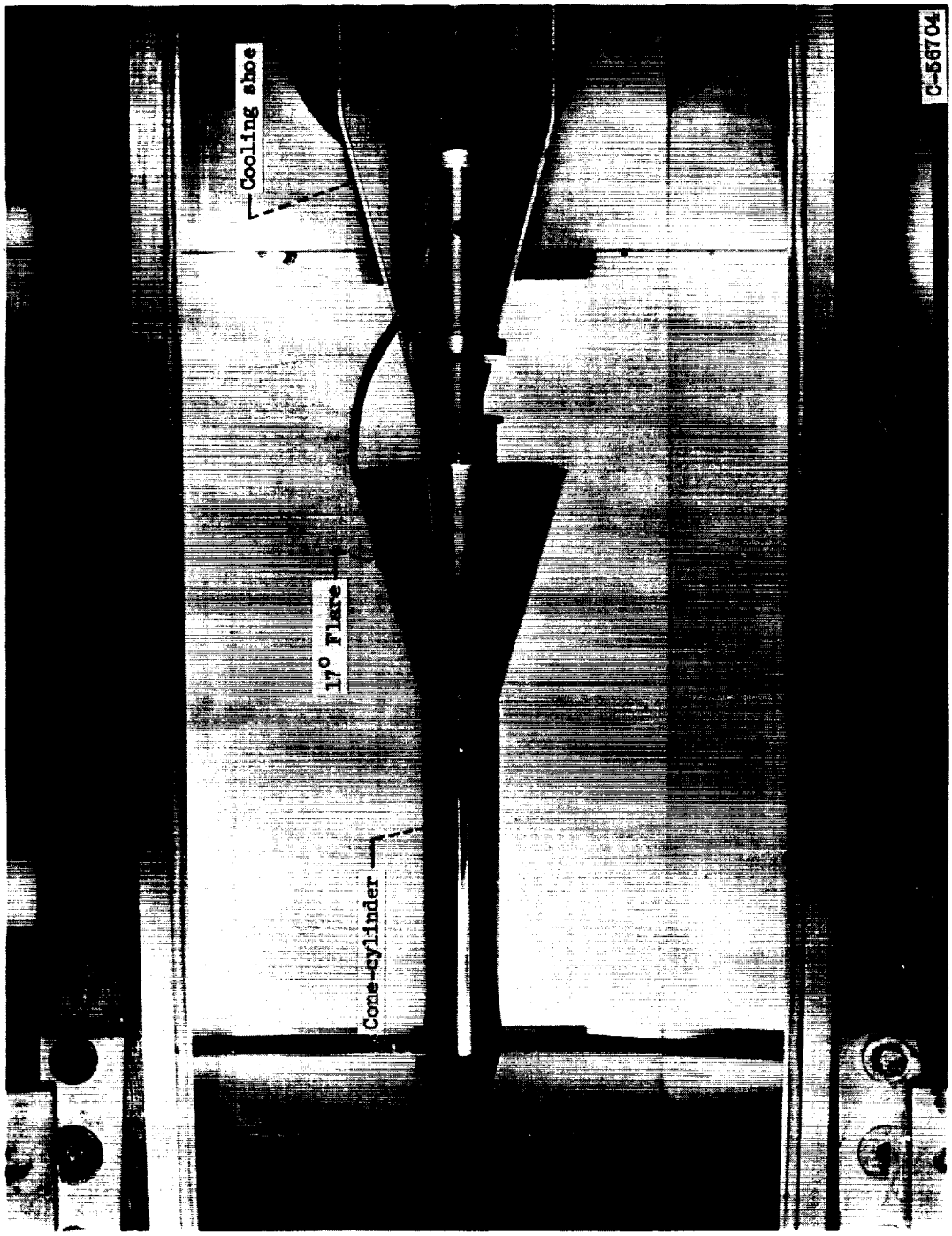

Figure 2. - Tunnel installation. Model in test position; cooling shoes retracted.

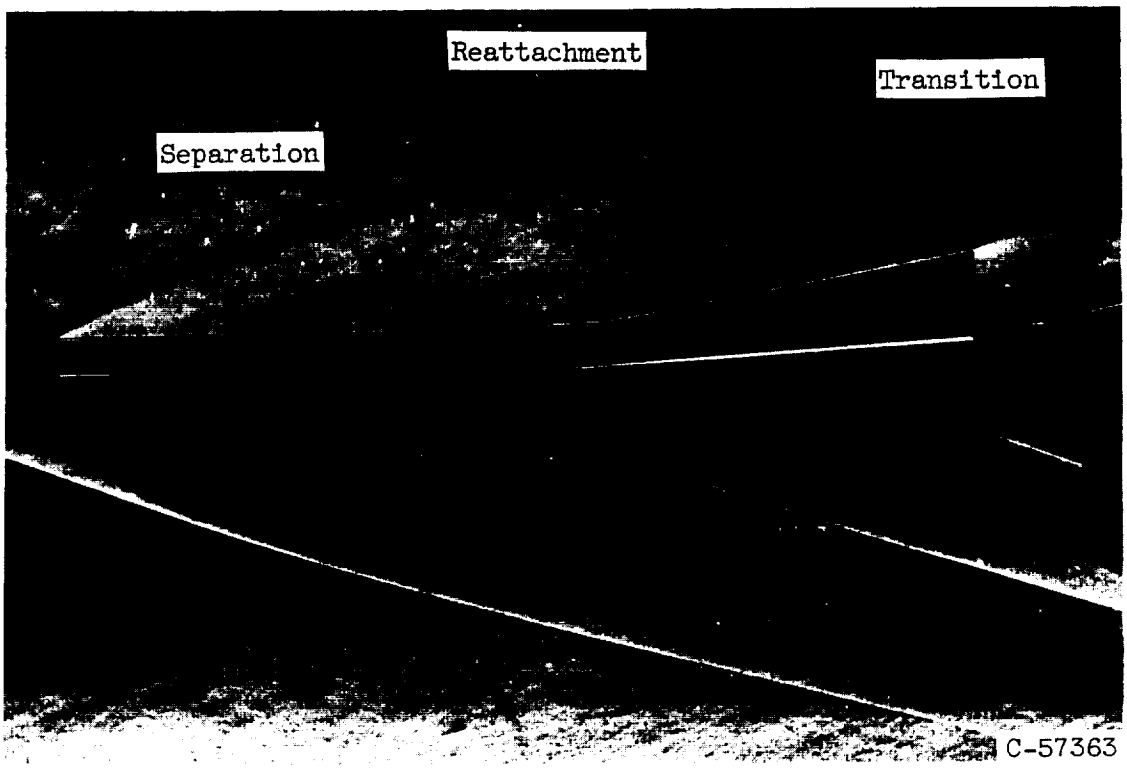

Figure 3. - Pure-laminar separation. Flare angle, 10°; unit Reynolds number, 1.9×10^{6} per foot; temperature ratio at separation $(T_w/T_t)_s$, 0.23; temperature ratio at transition $(T_w/T_t)_{TR}$, 0.40.

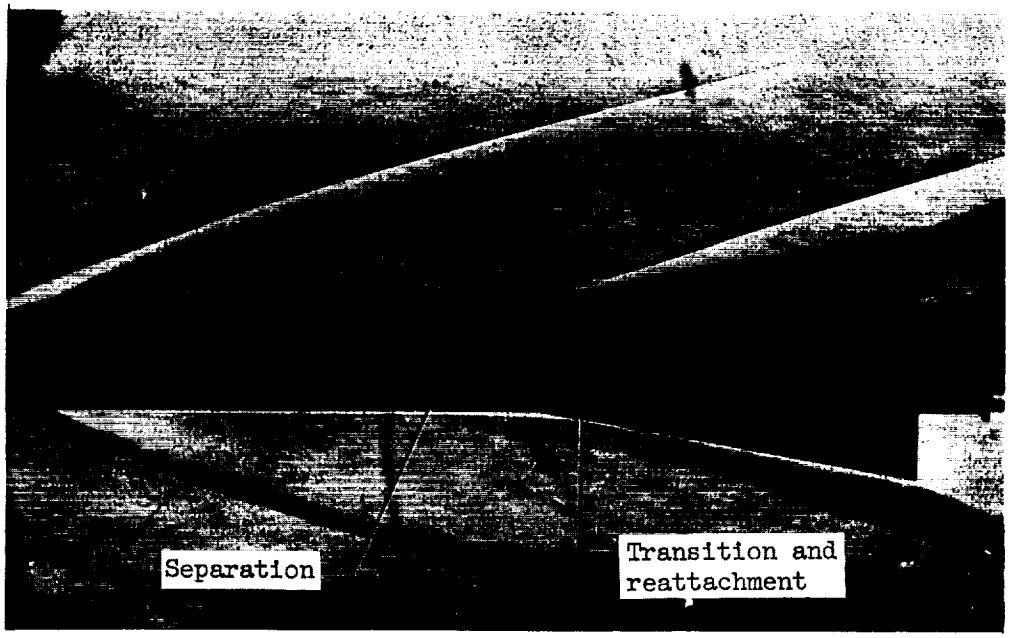

(a) Flare angle, 10°; unit Reynolds number, 5.4×10^{6} per foot; adiabatic wall.

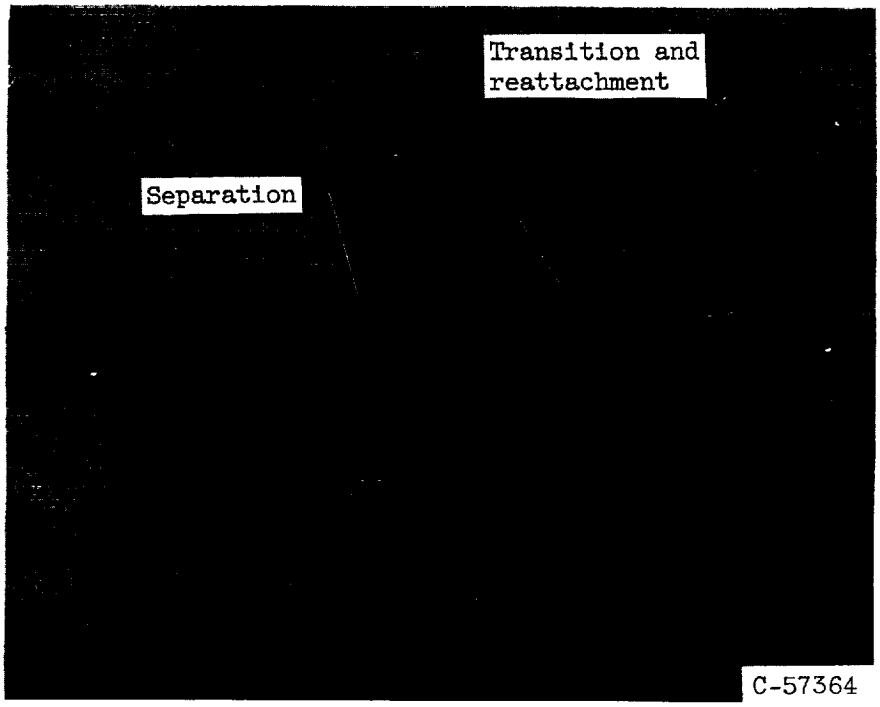

(b) Flare angle, 24°; unit Reynolds number, 5.4×10^{6} per foot; adiabatic wall.

Figure 4. - Transitional separation.

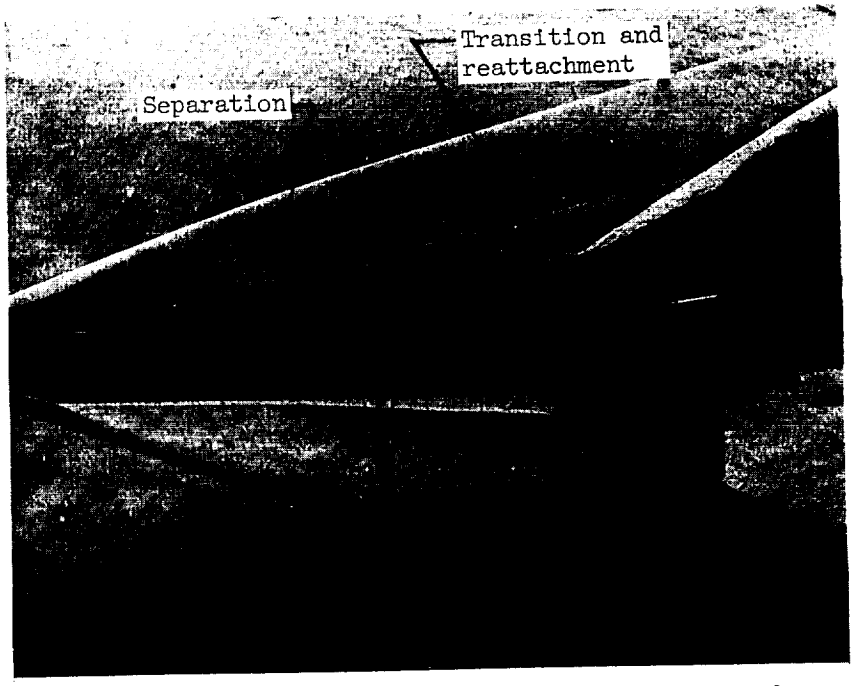

(c) Flare angle, 24°; unit Reynolds number, 2.6×10^6 per foot; adiabatic wall.

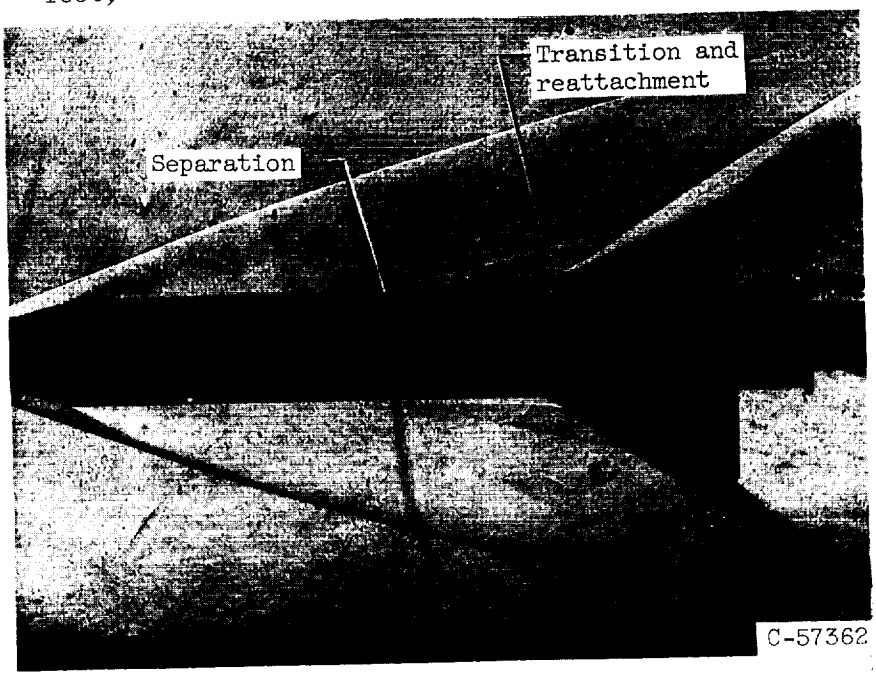

(d) Flare angle, 24°; unit Reynolds number, 2.6×10^6 per foot; temperature ratio at separation $(T_w/T_t)_s$, 0.18.

Figure 4. - Continued. Transitional separation.

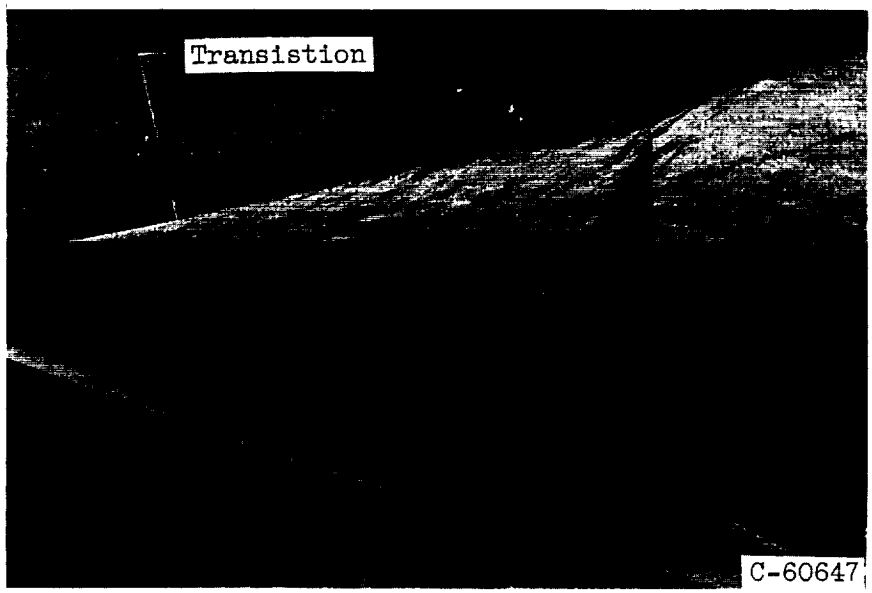

(e) Flare angle, 56°; unit Reynolds number, 5.4×10^{6} per foot; adiabatic wall.

Figure 4. - Concluded. Transitional separation.

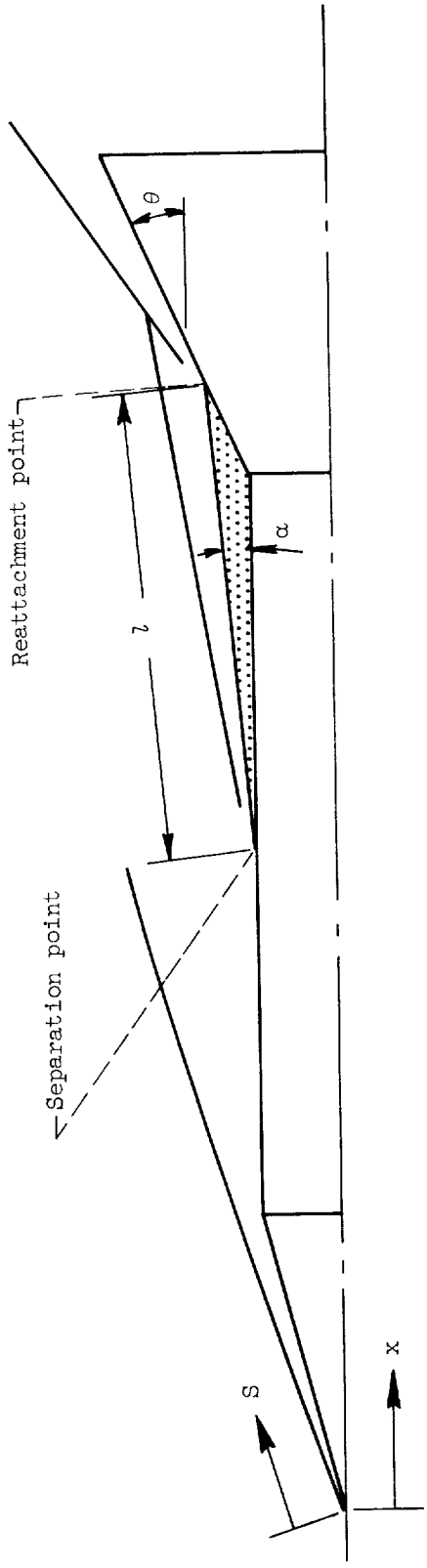

Figure 5. - Separation-geometry variables.

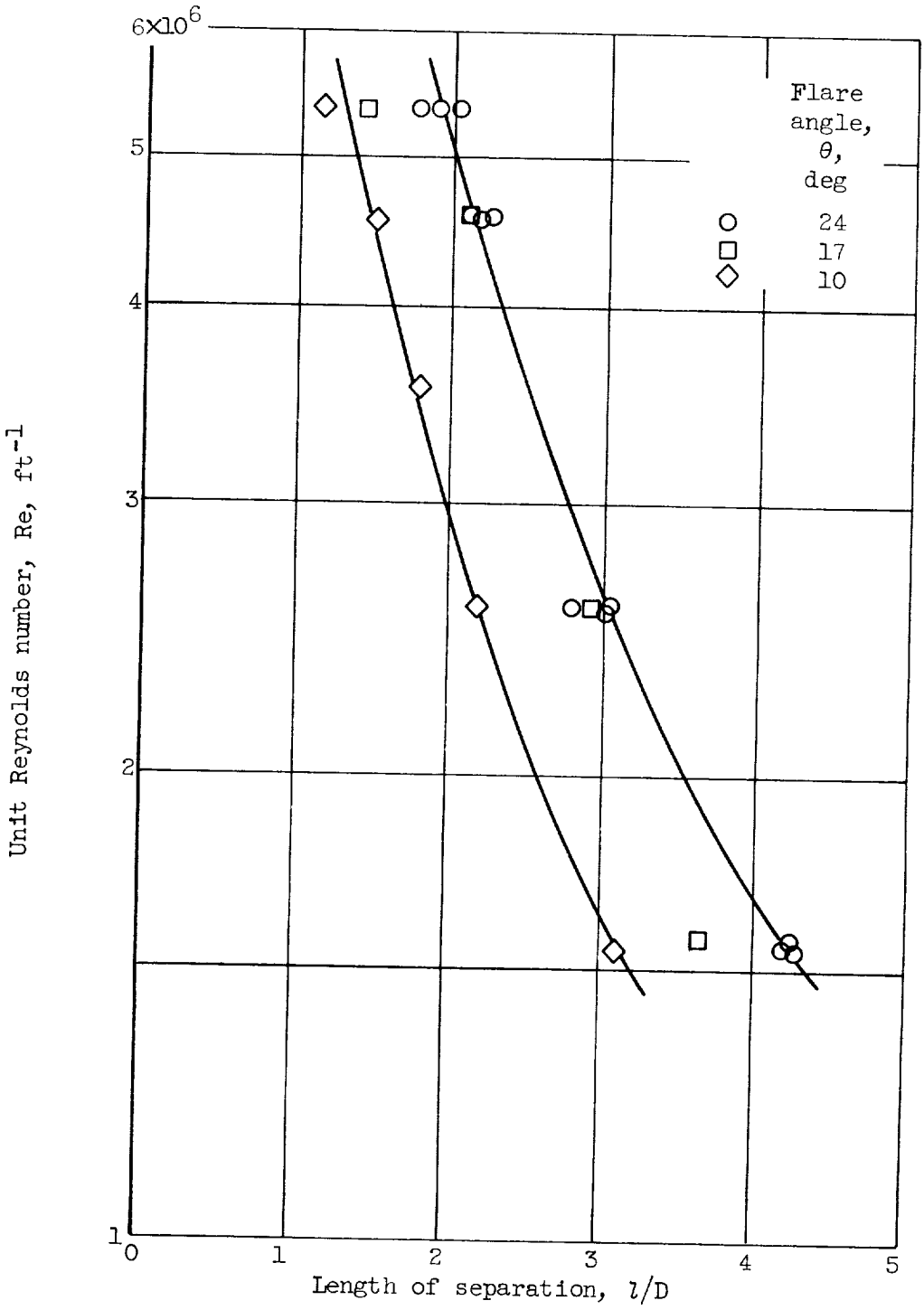

(a) Length of separation.

Figure 6. - Effect of unit Reynolds number and flare angle on separation geometry. Adiabatic wall.

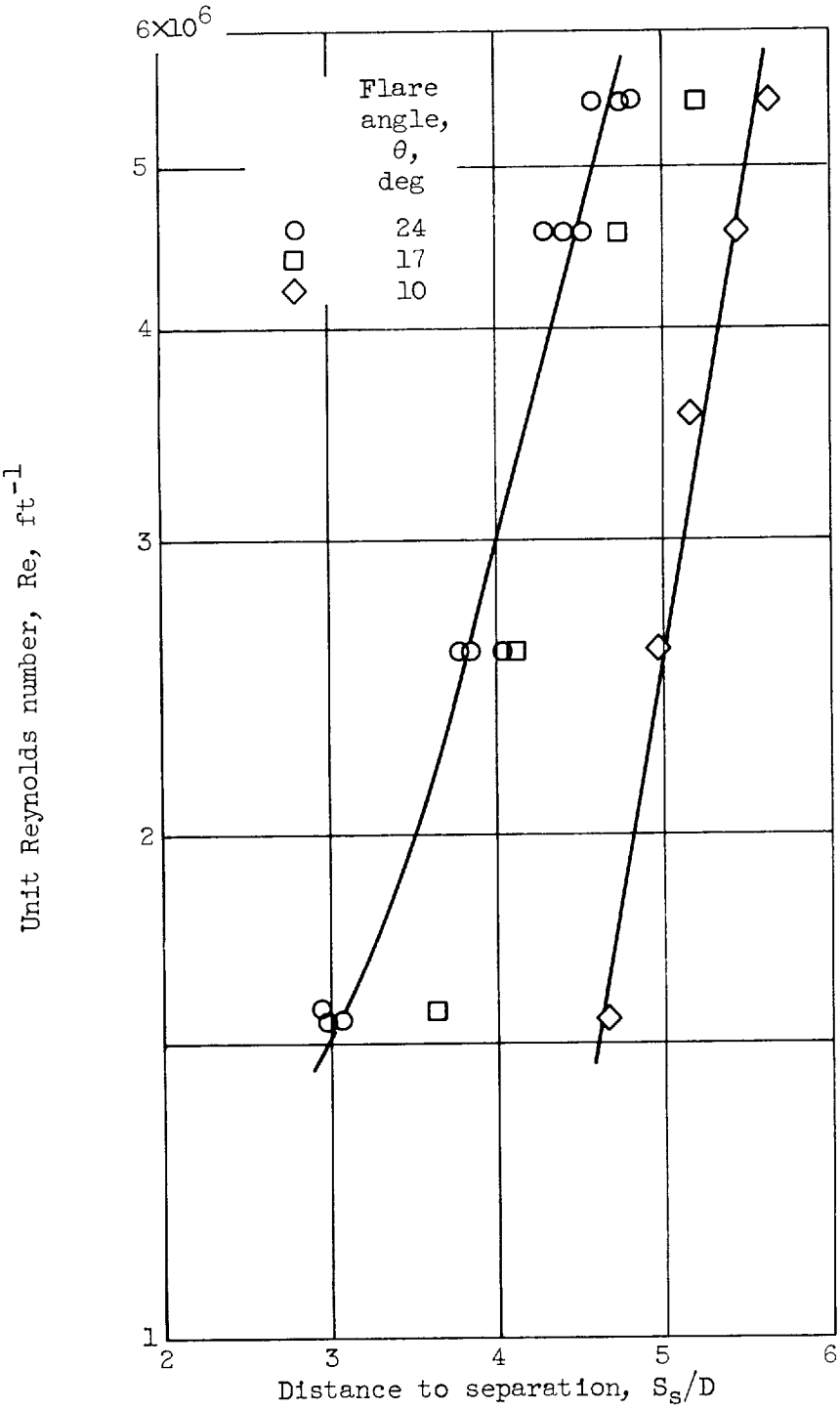

(b) Distance to separation.

Figure 6. - Concluded. Effect of unit Reynolds number and flare angle on separation geometry. Adiabatic wall.

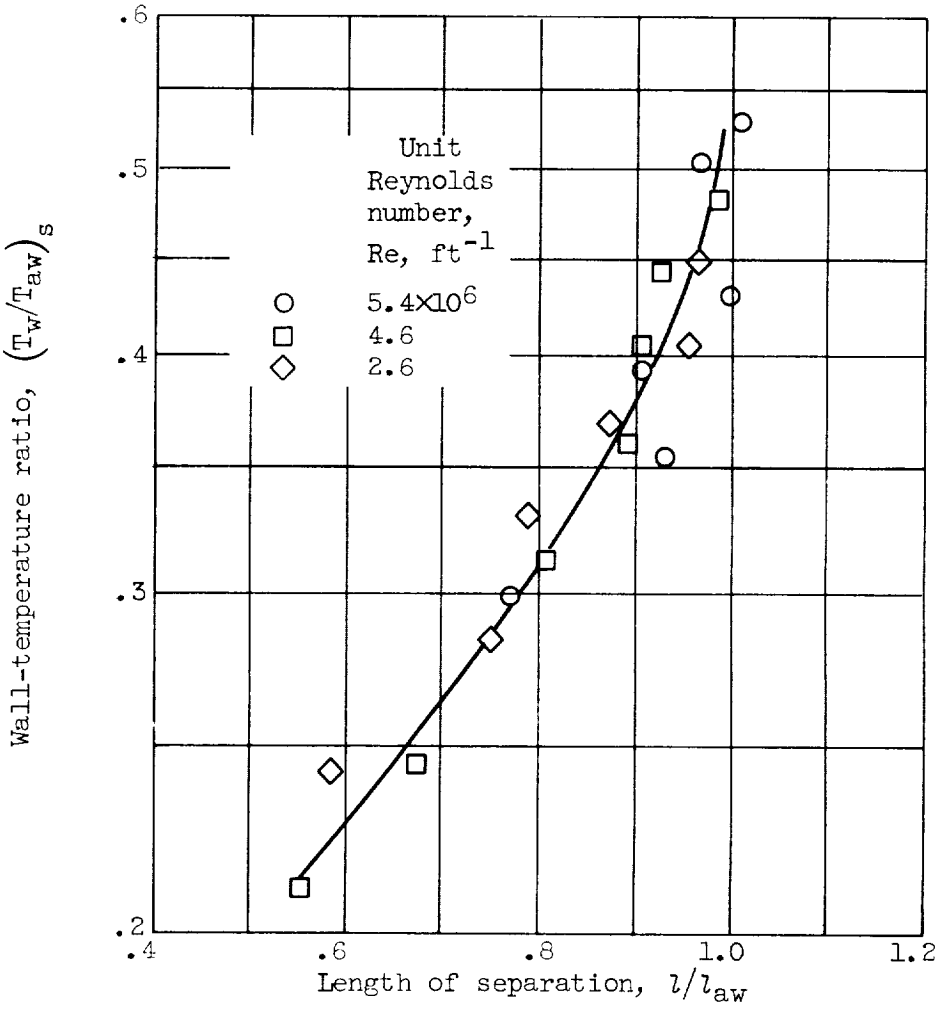

(a) Length of separation.

Figure 7. - Effect of wall cooling on separation geometry. Flare angle, 24°.

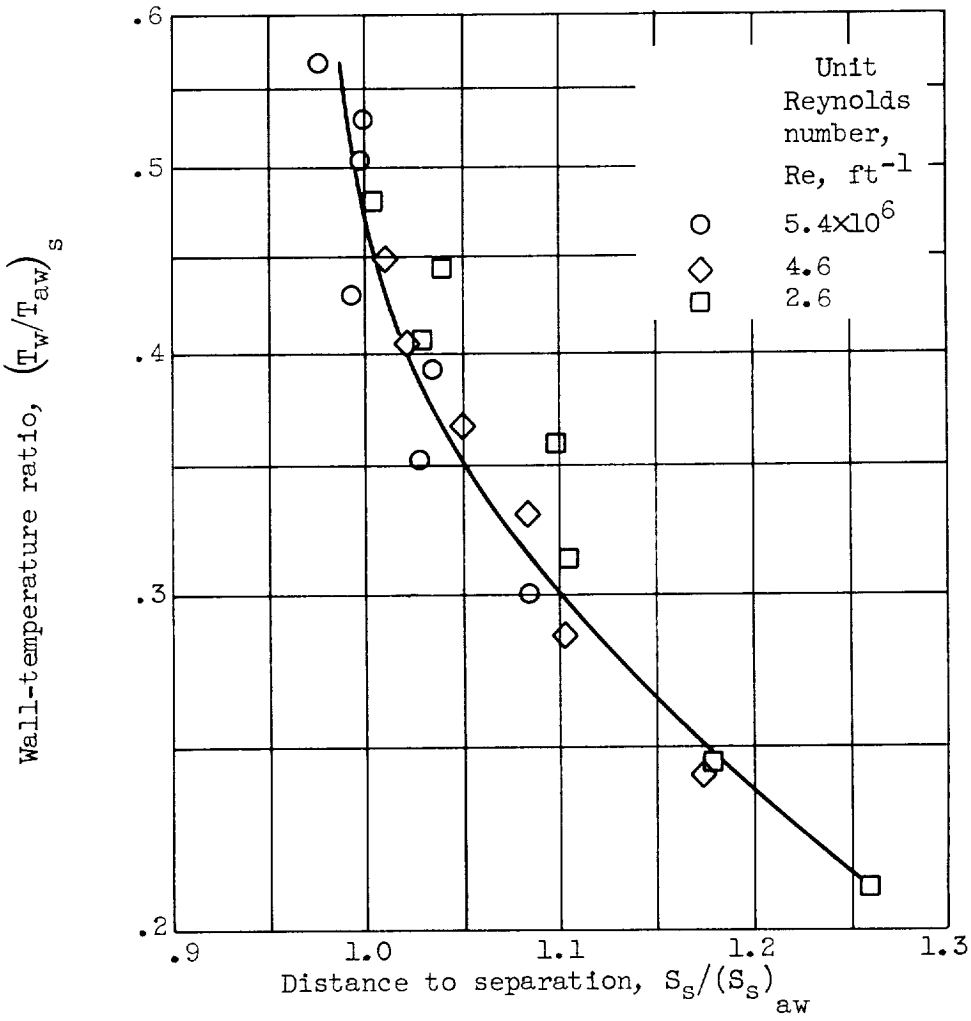

(b) Distance to separation.

Figure 7. - Concluded. Effect of wall cooling on separation geometry. Flare angle, 24°.

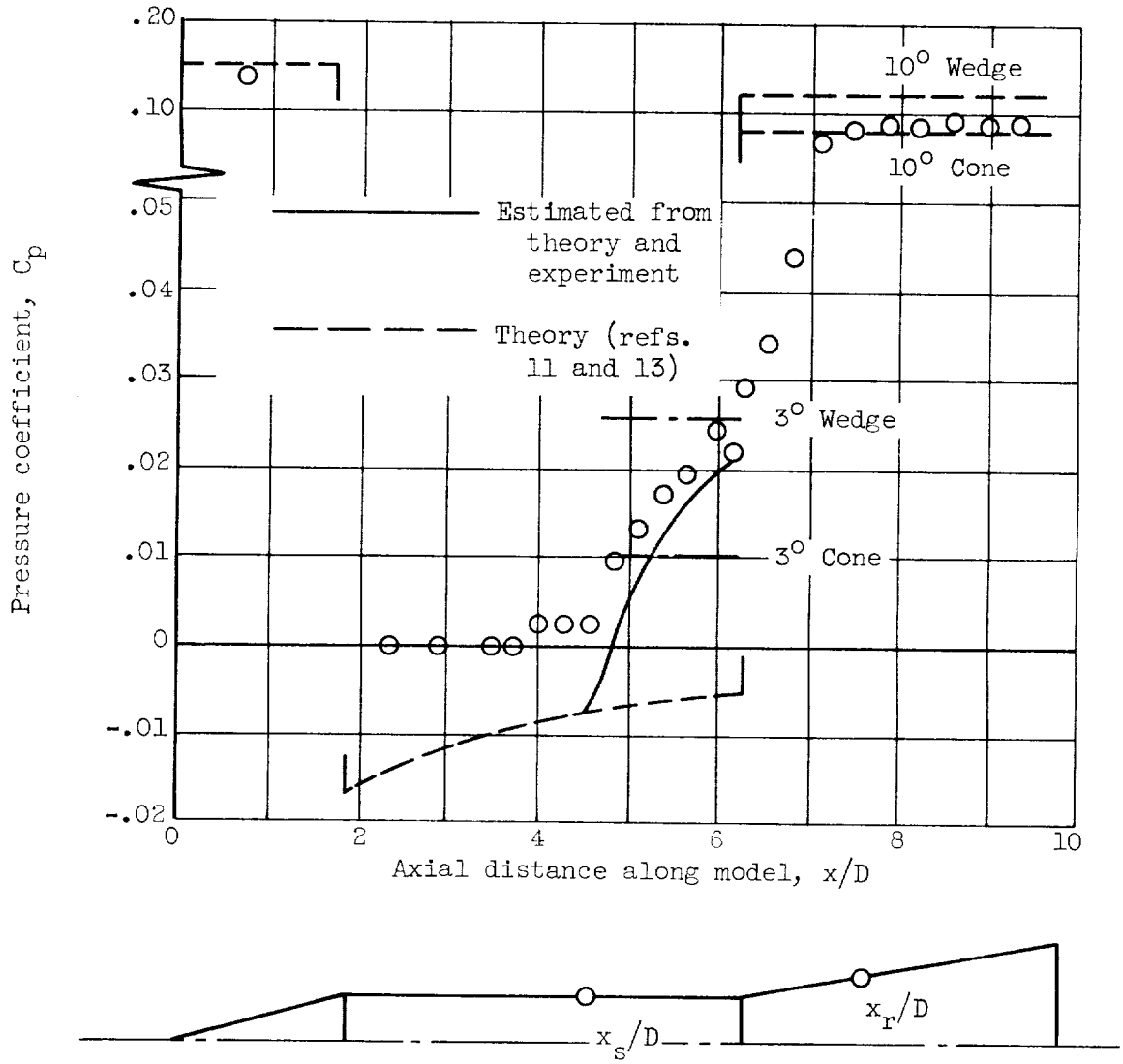

(a) Pure-laminar separation. Flare angle, 10°; unit Reynolds number, 1.6×10^6 per foot.

Figure 8. - Pressure distribution. Adiabatic wall.

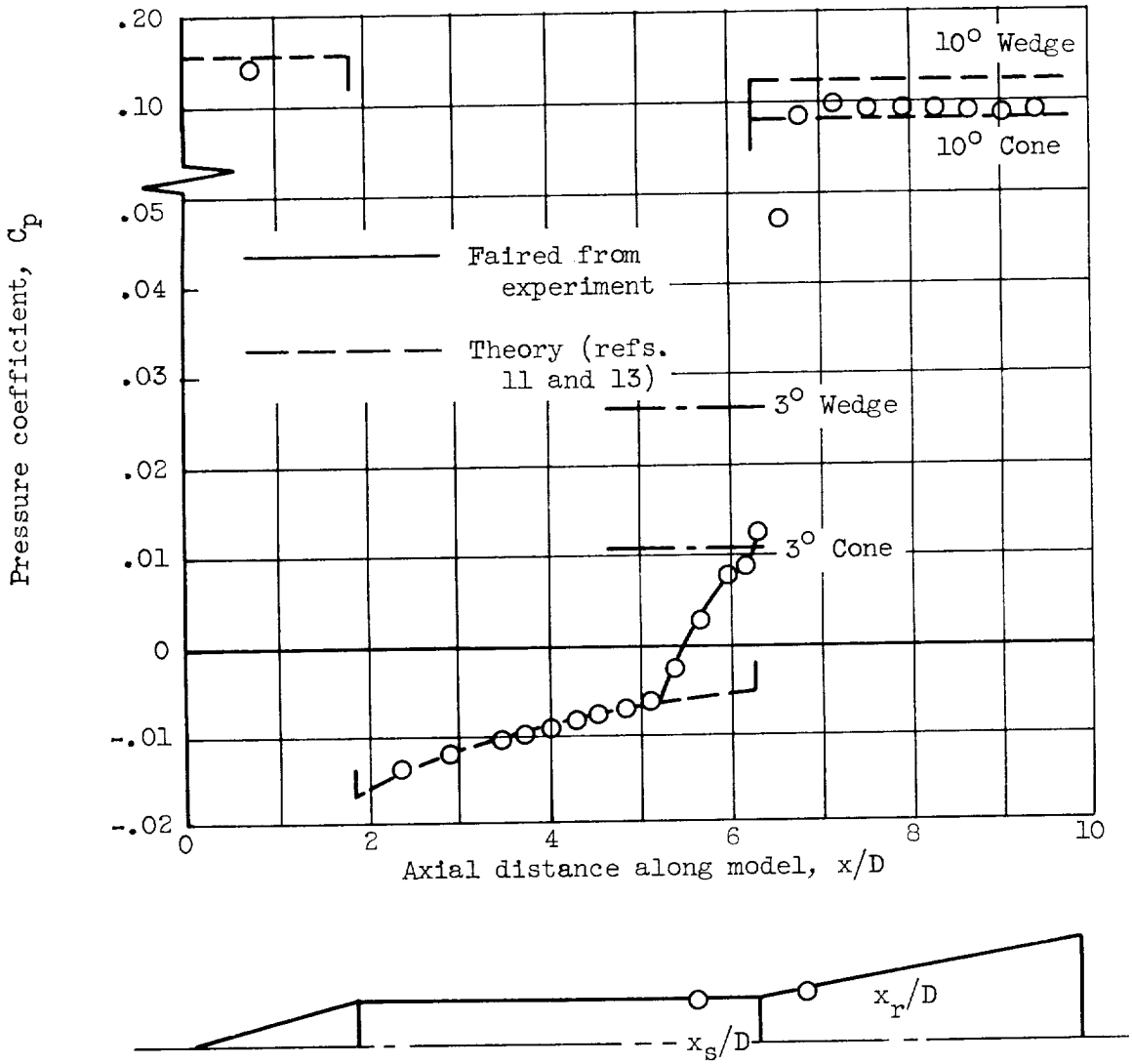

(b) Transitional separation. Flare angle, 10°; unit Reynolds number, 5.4×10^6 per foot.

Figure 8. - Continued. Pressure distribution. Adiabatic wall.

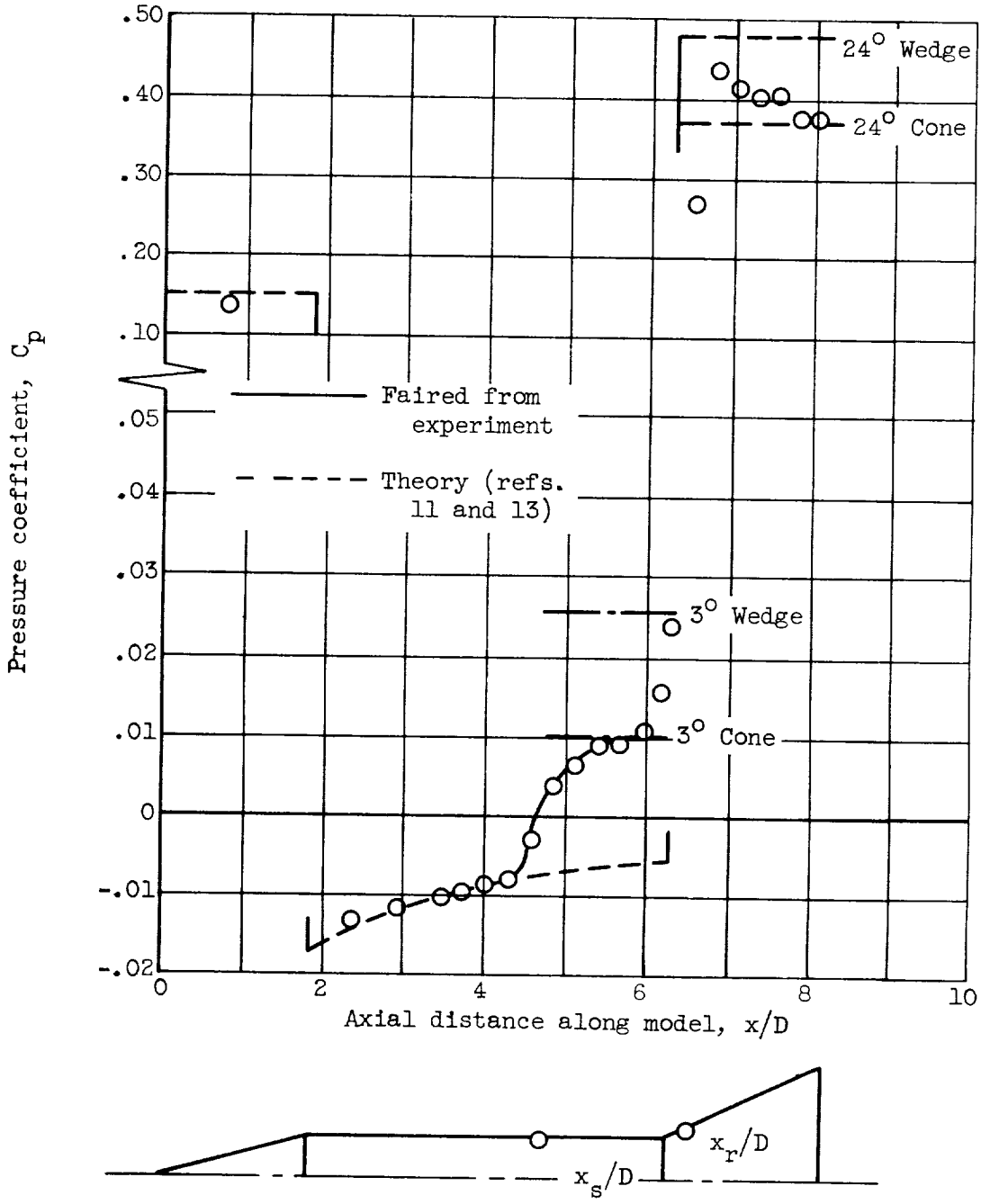

(c) Transitional separation. Flare angle, 24°; unit Reynolds number, 5.4×10^6 per foot.

Figure 8. - Continued. Pressure distribution. Adiabatic wall.

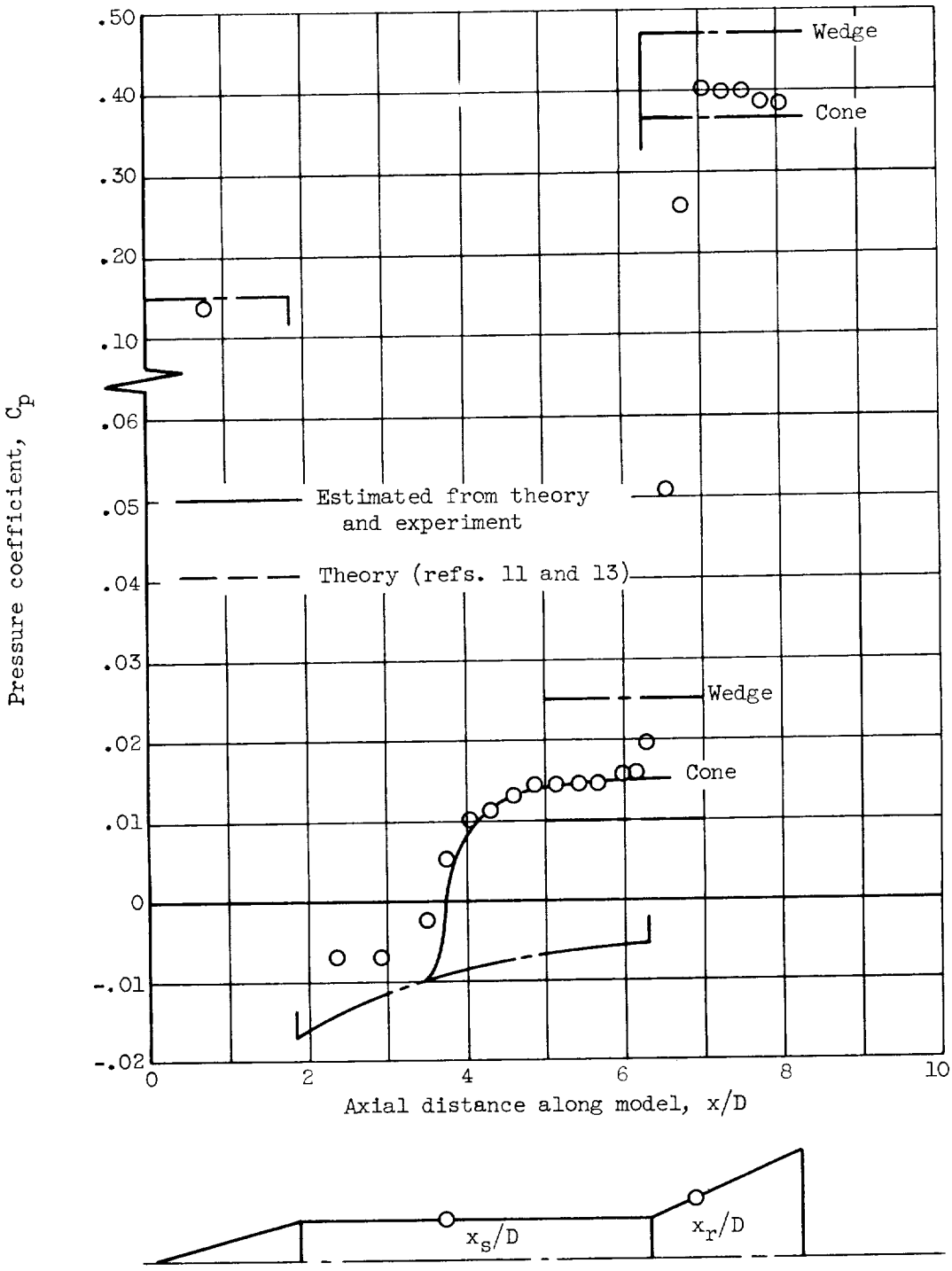

(d) Transitional separation. Flare angle, 24°; unit Reynolds number, 2.6×10^6 per foot.

Figure 8. - Continued. Pressure distribution. Adiabatic wall.

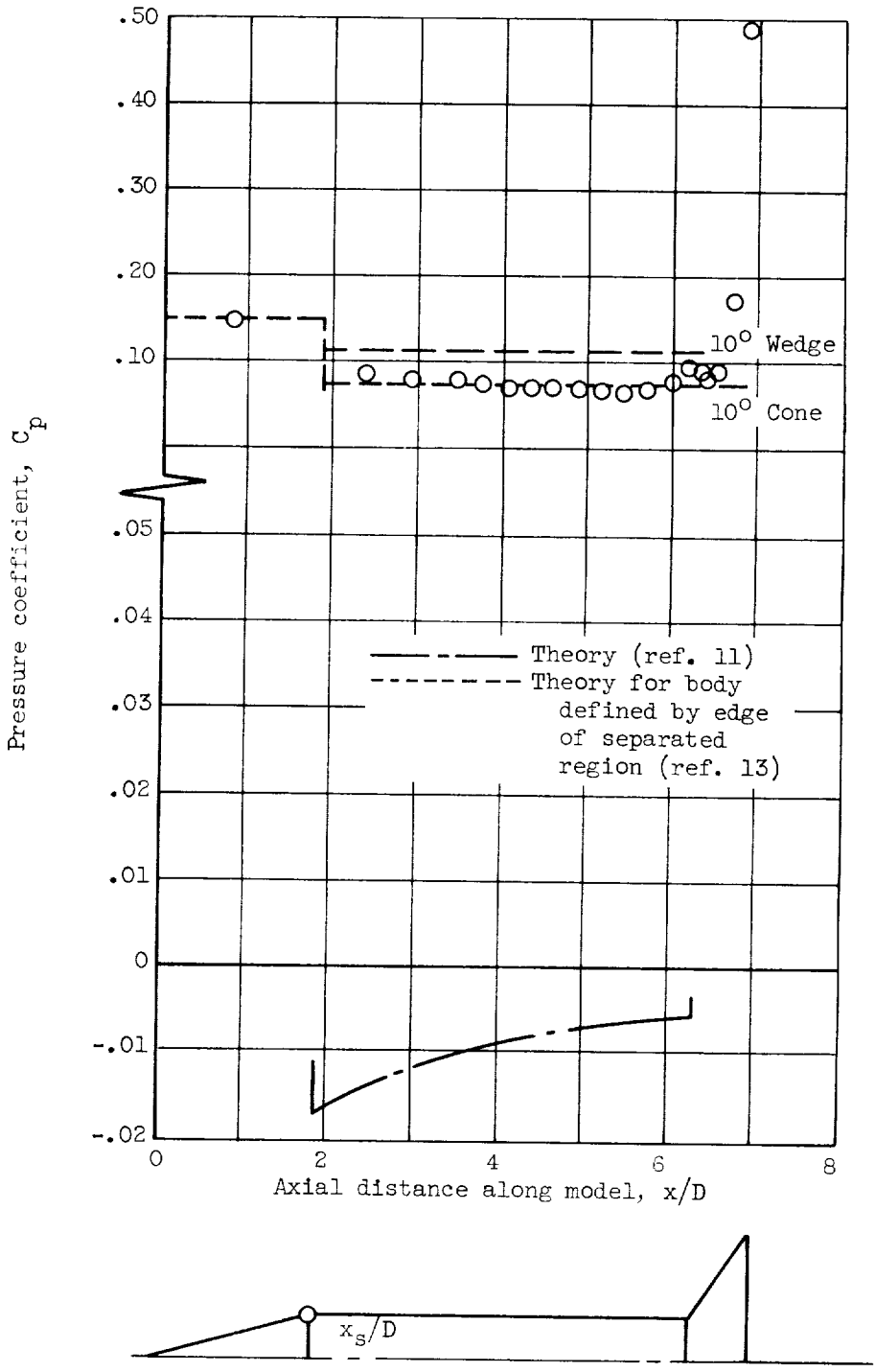

(e) Transitional separation. Flare angle, 56°; unit Reynolds number, 5.4×10^6 per foot.

Figure 8. - Concluded. Pressure distribution. Adiabatic wall.

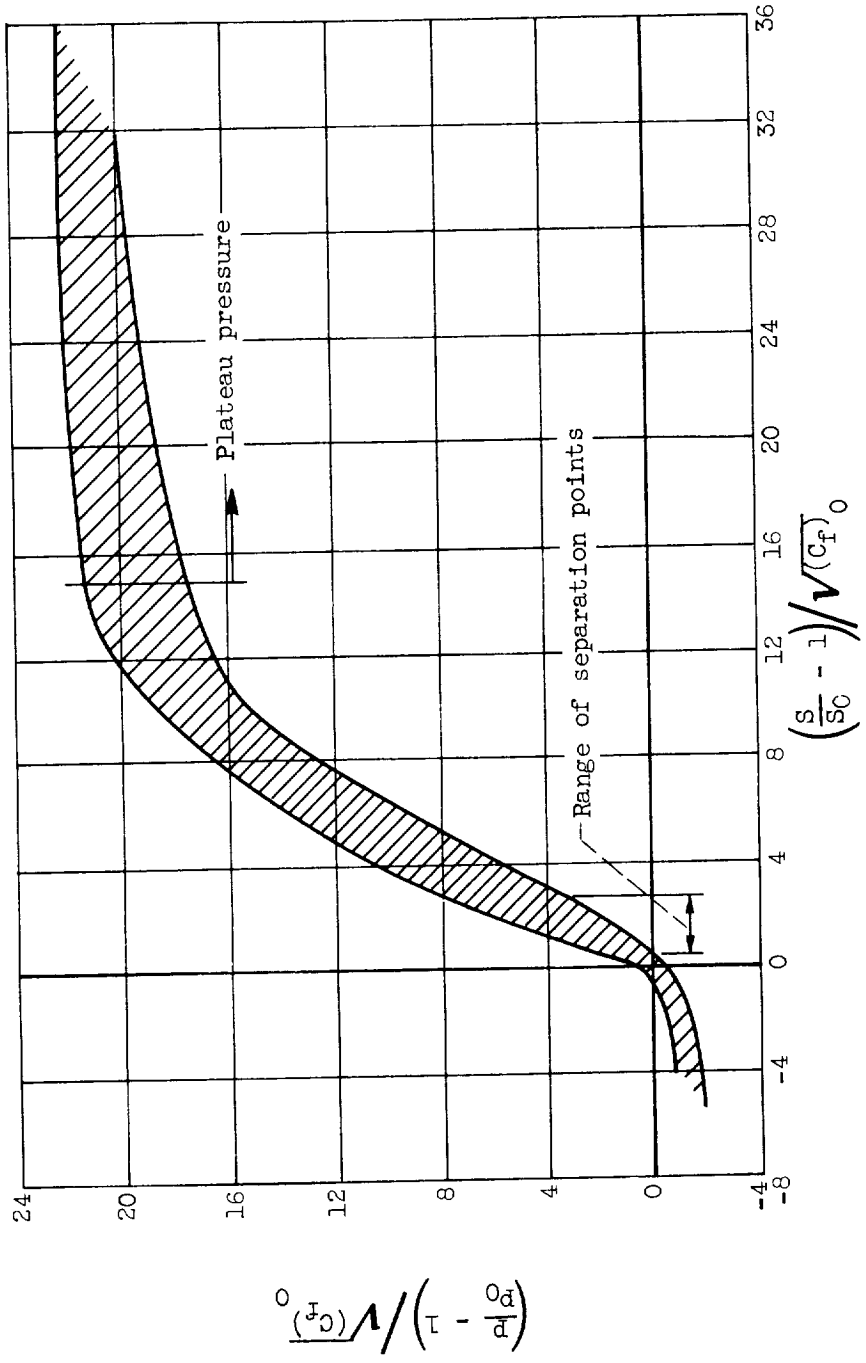

Figure 9. - Correlation of pressure distribution across separated region, pure-laminar and transitional separations. Flare angles, 10°, 17°, and 24°; unit Reynolds number, 1.6×10^6 to 5.4×10^6 per foot; adiabatic wall.

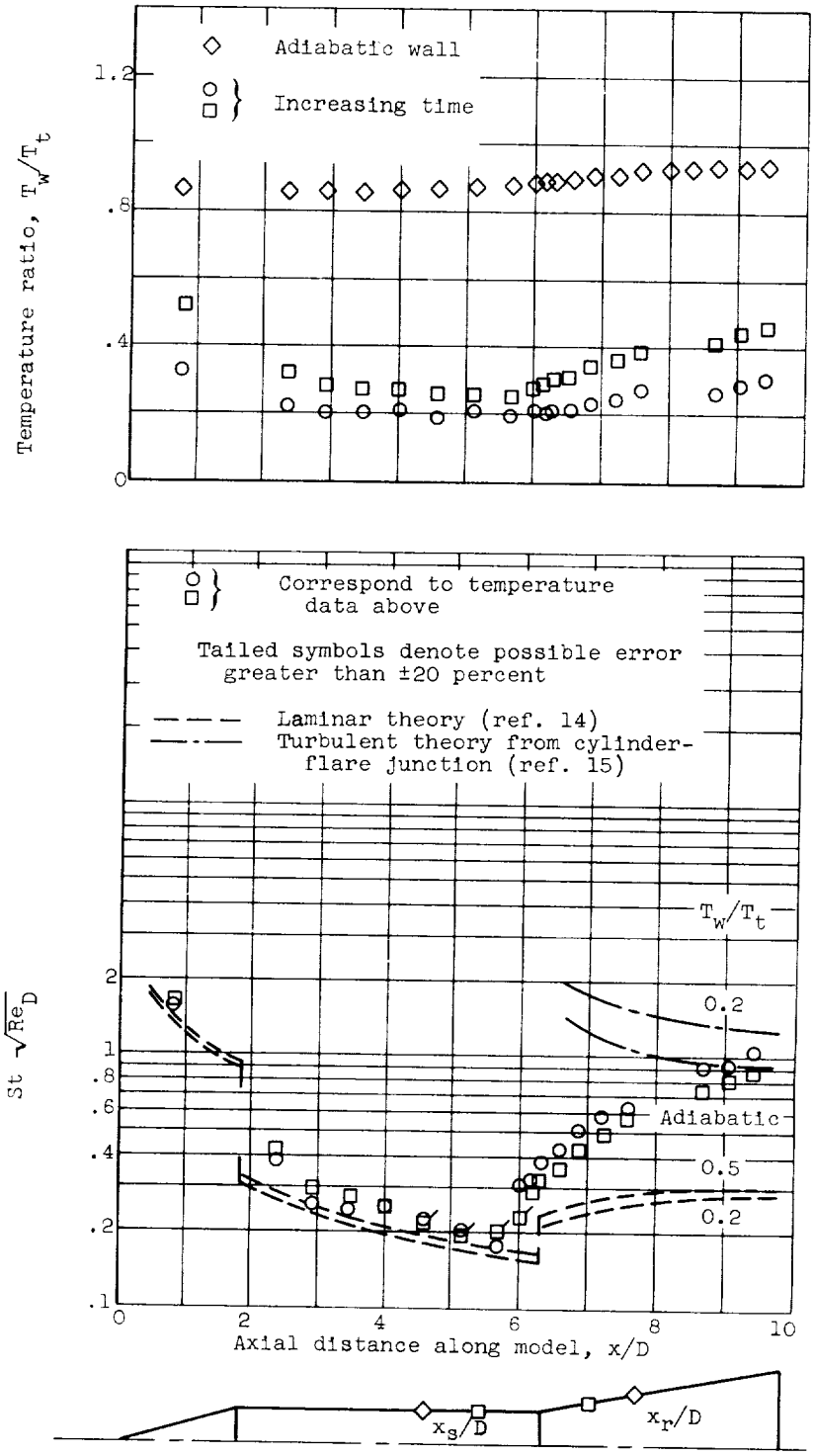

(a) Pure-laminar separation. Flare angle, 10°; unit Reynolds number, 1.6×10^6 per foot; Reynolds number based on body diameter, 0.24×10^6 per foot.

Figure 10. - Heat transfer.

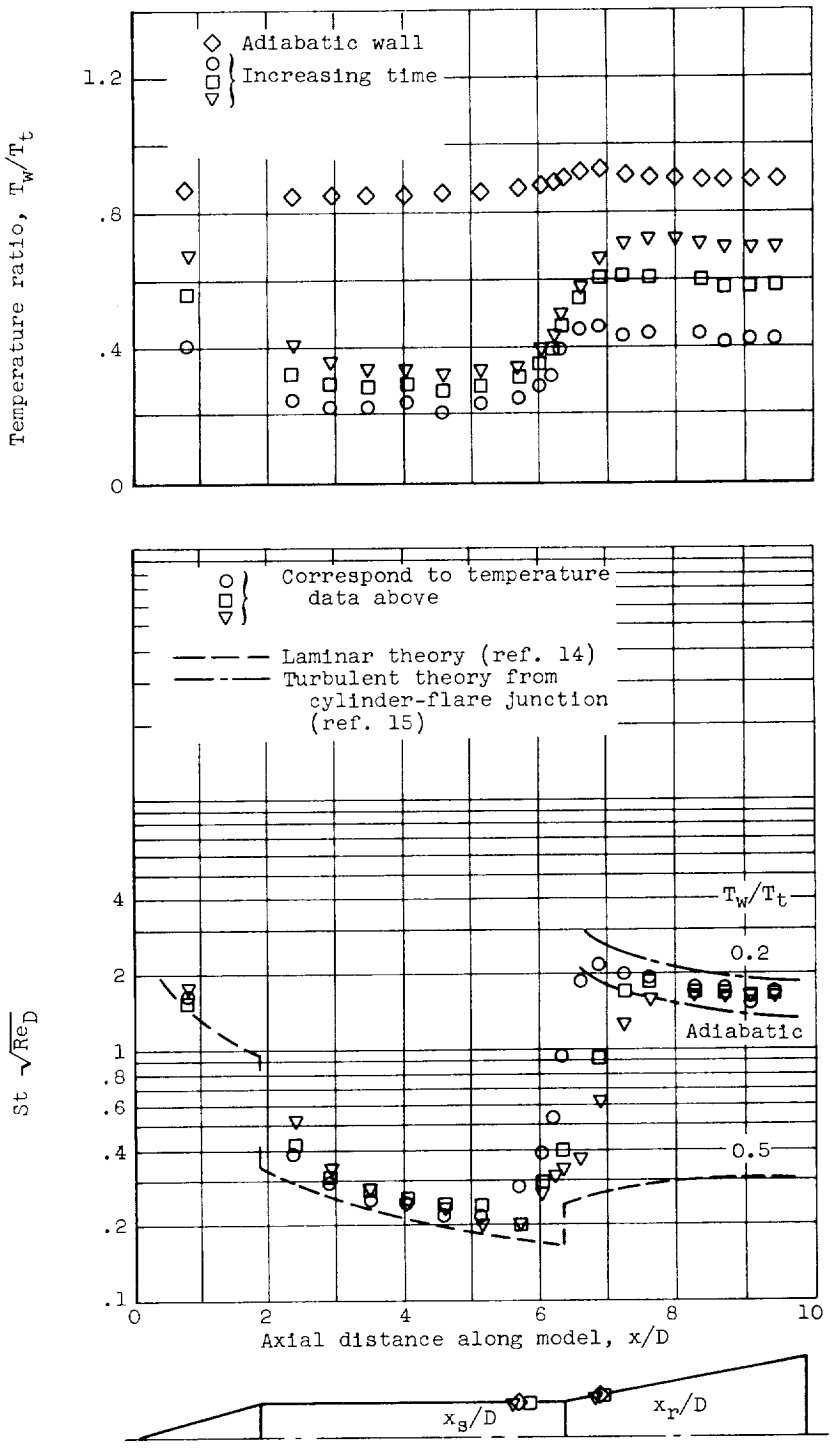

(b) Transitional separation. Flare angle, 10°; unit Reynolds number, 5.4×10^6 per foot; Reynolds number based on body diameter, 0.81×10^6 per foot.

Figure 10. - Continued. Heat transfer.

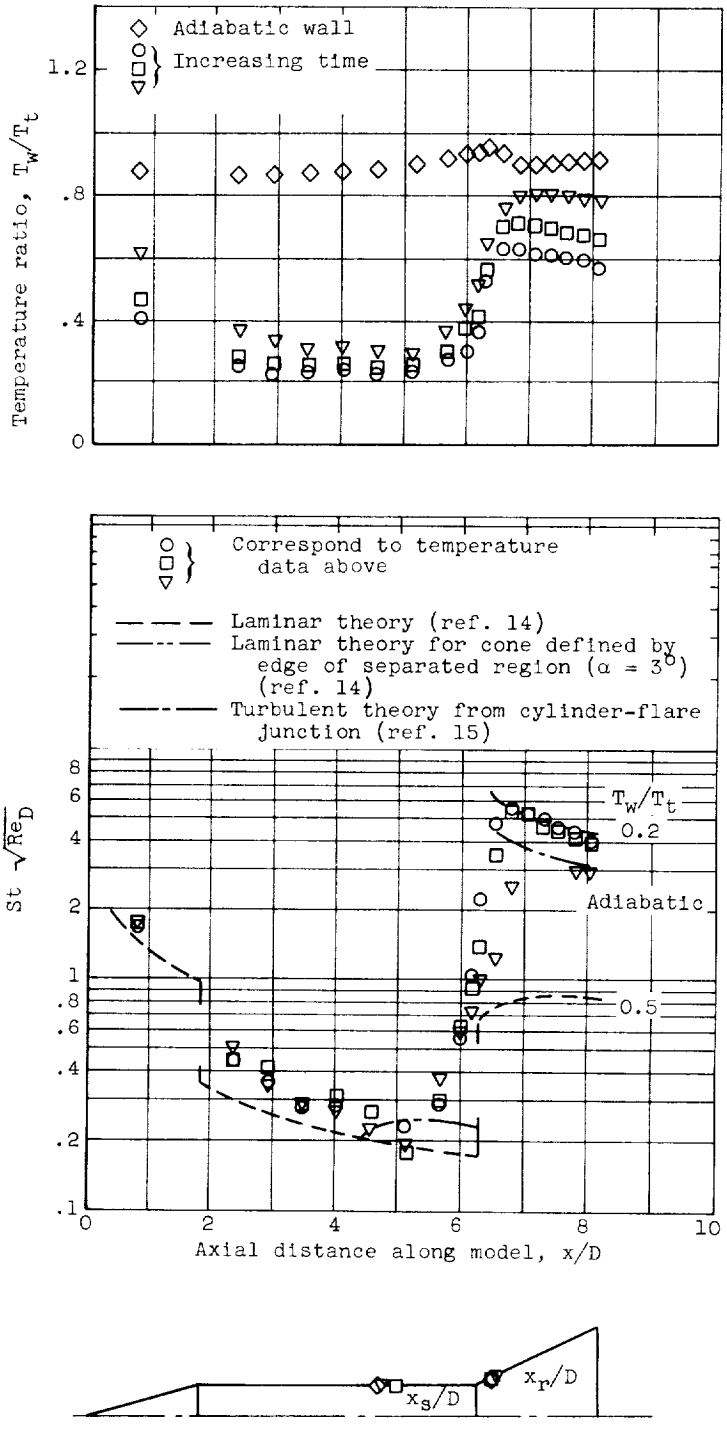

(c) Transitional separation. Flare angle, 24°; unit Reynolds number, 5.4×10^6 per foot; Reynolds number based on body diameter, 0.81×10^6 per foot.

Figure 10. - Continued. Heat transfer.

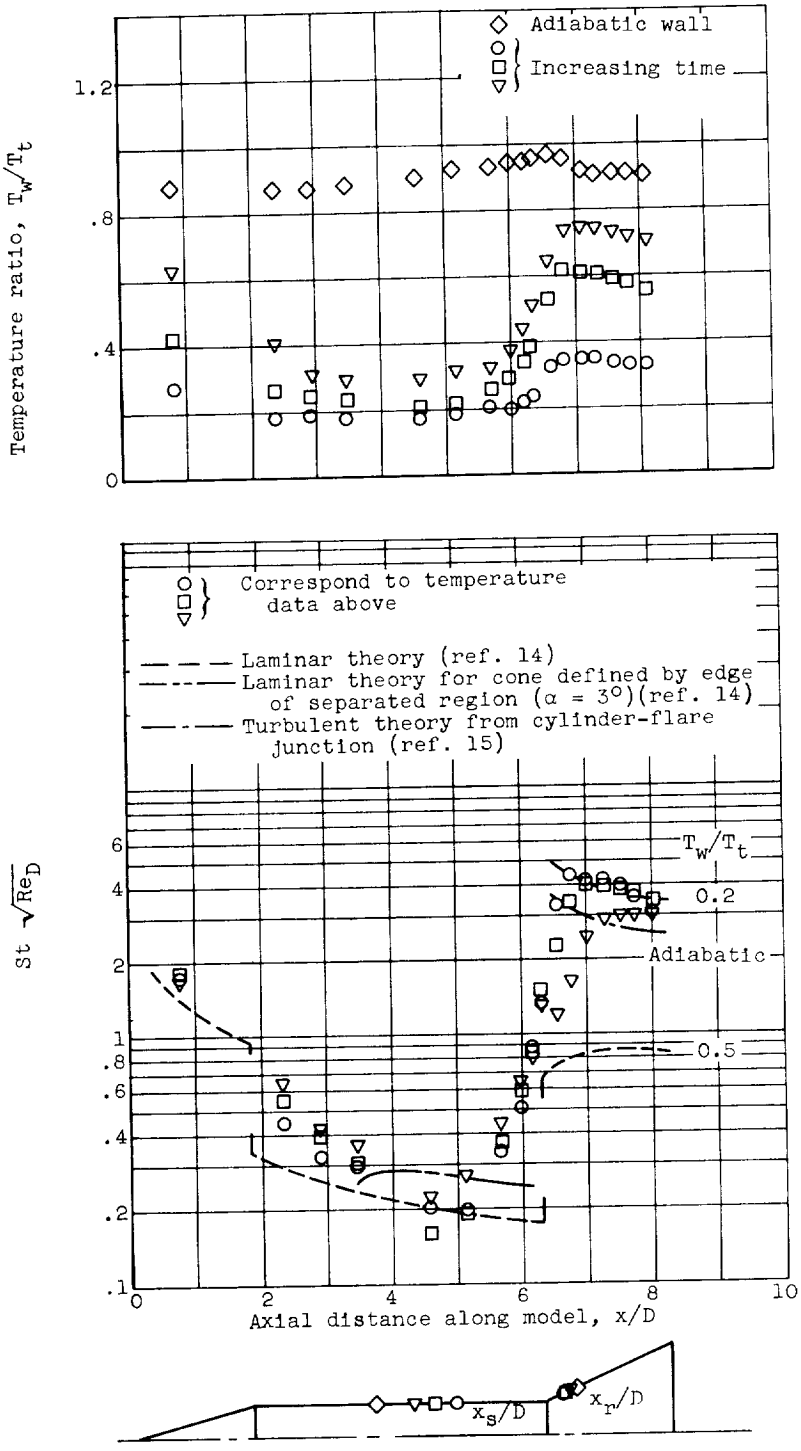

(d) Transitional separation. Flare angle, 24°; unit Reynolds number, 2.6×10^6 per foot; Reynolds number based on body diameter, 0.39×10^6 per foot.

Figure 10. - Continued. Heat transfer.

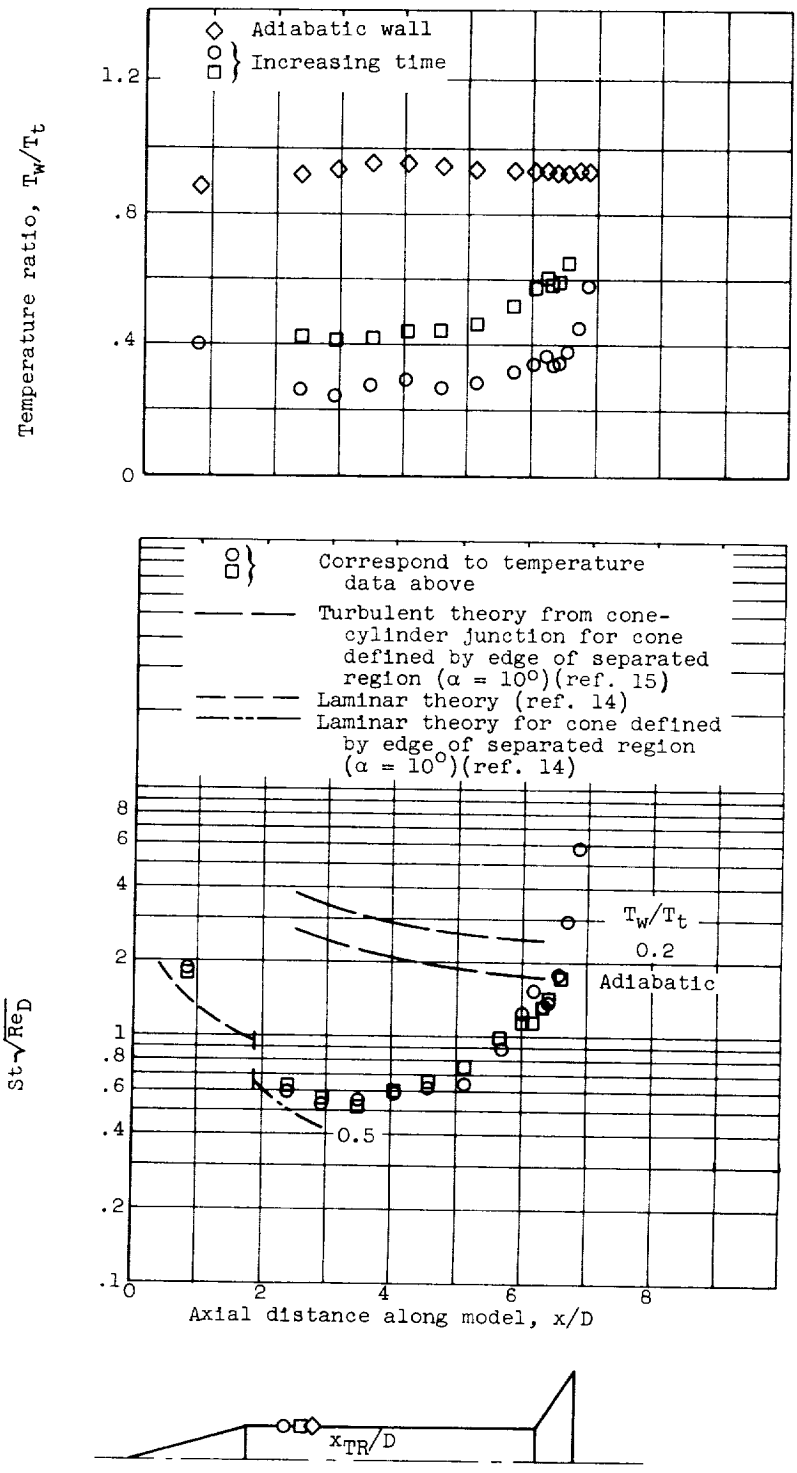

(e) Transitional separation. Flare angle, 24°; unit Reynolds number, 5.4×10^6 per foot; Reynolds number based on body diameter, 0.81×10^6 per foot.

Figure 10. - Concluded. Heat transfer.

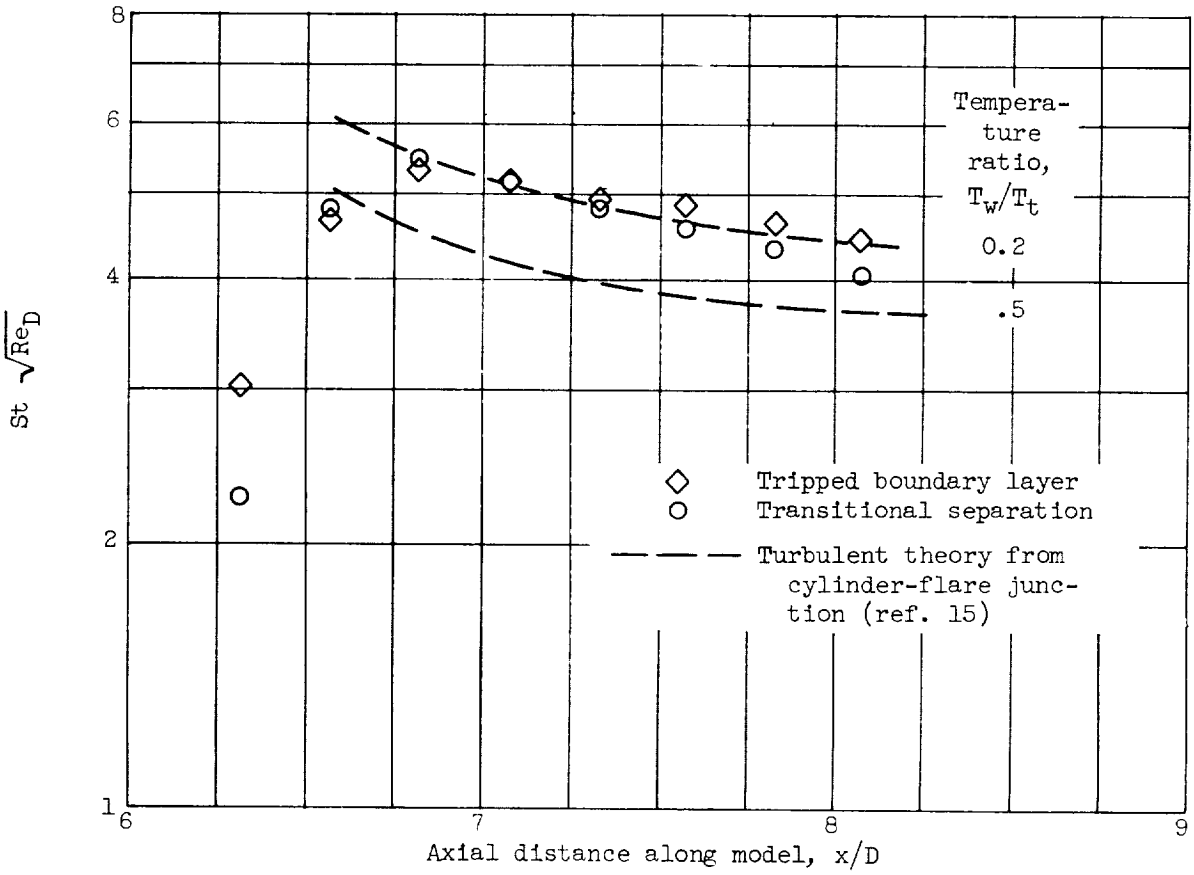

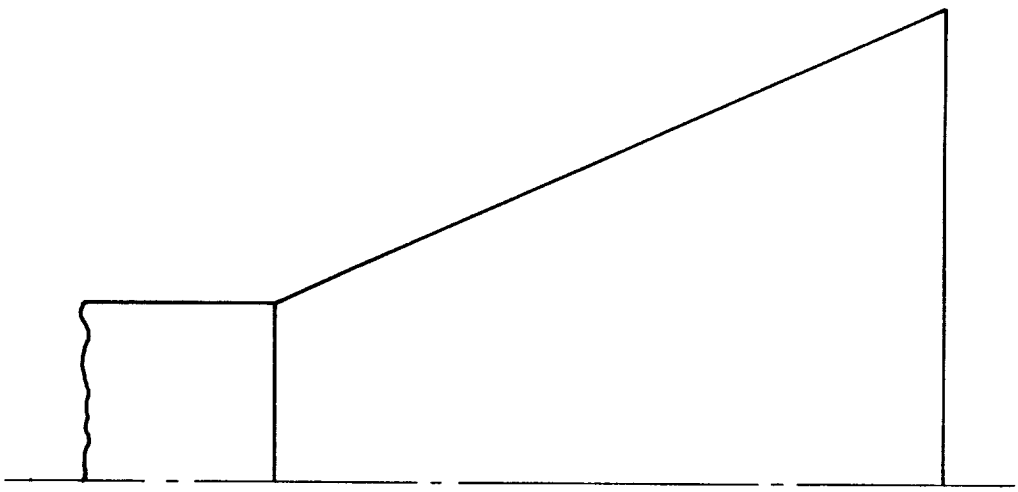

Figure 11. - Comparison of flare heat transfer for transitional separation and tripped boundary layer. Flare angle, 24°; unit Reynolds number, 5.4×10^6 per foot; Reynolds number based on body diameter, 0.81×10^6 per foot; experimental temperature ratio, 0.6.